Submission ID: [redacted]

In common with many of the residents impacted by the proposed Green Hill Solar farm development, I'm concerned that the installation of large numbers of solar arrays across agricultural land may alter surface water runoff characteristics thereby increasing the severity and/or frequency of flood events in areas already subject to flood risk.

The applicant's position on this aspect of flood risk, as documented in EX1/GH6.2.10_A and EX1/GH6.3.10.1_A, is that the presence of the panels does not result in a significant increase in surface water runoff. This position was echoed at Issue Specific Meeting ISH1 on 22 October 2025 when, in response to a question on this topic, the applicant's representative stated: "It's a common misconception that solar panels exacerbate flooding" (EVS2-008/EN010170-000696-GHS_ISH1_PART4, 1:26:51). At various junctures, the applicant has cited a research paper (Cook and McCuen, 2013) in support of their position. That research, conducted more than 12 years ago, uses mathematical models to simulate the impact of solar panels on surface water runoff behaviour.

A team at Virgina Tech College of Agriculture and Life Sciences is 2 years into a 6-year study to quantify stormwater-related impacts of utility-scale solar development. In the team's initial study paper "Preliminary Report on Runoff Characteristics from Utility-Scale Solar Sites" (Stewart, Mier-Valderrama, Hoben, Sample, Lee Daniels, 2025), it's noted by way of introduction that "… there continues to be much uncertainty regarding the extent to which development of utility-scale solar installations alters the magnitude and timing of stormwater delivery. There have been little-to-no measurements of surface runoff from utility-scale solar areas under real-world conditions …" (Stewart et al., 2025, p2). In an attempt to bridge this knowledge gap, the Virginia Tech study is measuring and quantifying precipitation and surface water runoff at a number of designated catchment sites, some of which contain existing solar installations while other comparable [reference] sites reflect pre-existing land use (e.g. agriculture).

The preliminary report published in November 2025 contains results and findings based on data gathered from January 2024 onwards.

The preliminary report Executive Summary contains the statement: "Our analysis showed that catchments within solar arrays tended to produce rapid, and at times substantial, amounts of surface runoff during storms. Based on the median and maximum storms measured at each site, catchments with solar arrays produced greater runoff volumes than reference catchments" (Stewart et al., 2025). The Results section of the report includes analysis and commentary based on statistics gathered for precipitation depth (P), runoff depth (Q), and runoff ratio (R), for instance "… at Site A the median storm (by Q) produced R values of 0.10-0.20 in the catchments with solar development (meaning that 10-20% of P was converted into measurable Q), versus 0.02 in the two reference catchments" (Stewart et al., 2025, p14).

The findings to date of the Virginia Tech study suggest that the presence of solar panels can materially affect runoff behaviour increasing both volume and rate of surface water runoff. I would ask that the ExA examines in detail the information afforded by the study and reviews whether this area of concern has been adequately addressed within the Green Hill Solar application.

The Virginia Tech study preliminary report can be found here:

[redacted]

I will also try to upload a PDF version of the same report.

Preliminary Report on Runoff Characteristics from Utility-Scale Solar Sites

Virginia Department of Environmental Quality Grant #17368

Ryan Stewart, Professor[1]
Luis Mier-Valderrama, Graduate Research Assistant[1]
John Hoben, Research Scientist[1]
David Sample, Professor[2,3]
W. Lee Daniels, Professor Emeritus[1]

[1]School of Plant and Environmental Sciences, [2]Biological Systems Engineering;
[3]Hampton Roads Agricultural and Research Extension Center;
College of Agriculture and Life Sciences;
Virginia Polytechnic Institute and State University (Virginia Tech)

November 22, 2025

Executive Summary

Utility-scale solar sites are being developed across the state of Virginia, yet there is considerable uncertainty regarding the amount and timing of stormwater generated from these installations. It is similarly unknown if the parameters used to design stormwater detention basins and ponds, including curve numbers (CNs) and times of concentration, are being appropriately specified. With funding from the Virginia Department of Environmental Quality (VDEQ), in 2023 we began a six-year study to quantify and interpret stormwater generation from utility-scale solar sites across the state. This report presents preliminary results from the initial stage (1-2 years) of stormwater monitoring associated with that project, focusing on three utility-scale solar sites in Virginia.

The three sites (hereafter deemed Sites A, B, and C) were built between one and eight years prior to the start of monitoring, and thus were designed under VDEQ stormwater management guidelines that were in effect prior to December 2024. At each site we measured precipitation and surface runoff from small catchments developed with solar infrastructure and from comparable nearby reference catchments that represent pre-existing land uses (e.g., agriculture, forestry). The dataset to date included 76 identified storms at Site A, 39 storms at Site B, and 41 storms at Site C. Many storm events produced measurable runoff in the monitored catchments, which were used to calculate 1) rainfall-runoff ratios, 2) time of concentration values as the lag between effective precipitation and surface runoff, and 3) best-fit CNs for each monitored catchment based on runoff response metrics across storms.

Our analysis showed that catchments within solar arrays tended to produce rapid, and at times substantial, amounts of surface runoff during storms. Based on the median and maximum storms measured at each site, catchments with solar arrays produced greater runoff volumes than reference catchments. The time of concentration values at Site A were similar between catchments with solar panels and a reference catchment containing a row-crop field (means of 1.2-2.1 h), and all were much shorter than the time of concentration measured in a nearby reference catchment with a mixture of grass and forest cover (mean of 3.5 h).

Many individual storms generated runoff from solar areas that corresponded to CN values > 80, though some large storms did not produce appreciable runoff. Apparent CNs, which were fit to each site using a subset of the storm record, varied considerably between catchments. At Site A, best-fit CNs ranged from 76.8 to 84.3, which were similar to or greater than the best-fit CNs of the reference catchment containing a corn-soybean field (CN = 75.5) and greater than the reference catchment with a grass-forest mixture (CN = 61.8). Both catchments with solar panels at Site B and one of three paneled catchments at Site C had best-fit CNs > 85, whereas a reference soybean field in Site B had a best-fit CN of 67.5. These results imply that solar development is increasing stormwater runoff volumes relative to pre-development conditions across a range of sites and storm events.

This preliminary report will be followed by a second assessment with two more years of data (anticipated by November 2027) and a final report that will summarize the entire dataset and provide recommendations aimed at enhancing stormwater management at these sites (anticipated by November 2029). Those reports will be expanded to include data from 2-3 additional sites, including two that have or will be constructed during the monitoring period. We are complementing stormwater quantity data by collecting stormwater samples during storms, which are being analyzed for important water quality parameters such as total phosphorus, total nitrogen, and total suspended solids. We are also in the process of characterizing soil properties, such as bulk density and permeability, and vegetation at the sites, all which are important factors in runoff responses. These data will ultimately be compared against model parameters and assumptions used in the site design process, with the aim of enhancing stormwater management at utility-scale sites. We anticipate these future reports will provide better clarity on issues such as how stormwater quantity and quality are affected by factors such as the degree of disturbance during construction, the orientation of panels relative to the ground surface, and the relative imperviousness of the panels themselves.

Index

List of Terms

A – catchment area (acre, ha, or m^2)
CN – curve number
h – water stage (ft or mm)
I_a – initial abstraction (in or mm)
P – total precipitation during a storm event (mm or in)
P^* – total effective precipitation during a storm event; $P^* = Q$ (mm or in)
p – precipitation rate (in/h or mm/h)
p^* – effective precipitation rate (in/h or mm/h)
Q – runoff depth (mm or in)
q – volumetric discharge (cfs, cfm, or m^3/s)
$q_{adjusted}$ – surface runoff adjusted by removing any pre-event flow (cfs, cfm, or m^3/s)
q_{depth} – surface runoff rate as an equivalent depth (mm/h)
$q_{minimum}$ – minimum runoff measured during event, used for flow adjustment (cfs, cfm, or m^3/s)
$q_{threshold}$ – threshold flow value used to identify start and end of runoff events (cfs, cfm, or m^3/s)
$q_{stormflow}$ – volumetric surface runoff rate (cfs, cfm, or m^3/s)
R – ratio of the total amount of surface runoff to precipitation; $R = Q/P$
S – storage in the catchment (in or mm)
t – time, typically for each storm event as time since rainfall begins (h)
T_c – time of concentration; $T_c = t_{qc} - t_{pc}$ (h)
$t_{mid,i}$ – time of the midpoint of timestep interval i (h)
t_{p0} – start of precipitation (h)
t_{pc} – time of the centroid of effective precipitation (h)
t_{pk} – time of peak surface runoff (h)
t_{qc} – time of the centroid of surface runoff (h)
t_{qe} – end of surface runoff (h)
t_{q0} – start of surface runoff (h)
V_{runoff} – total volume of surface runoff during a storm event (m^3)
λ – initial abstraction ratio; $\lambda = I_a/S$
ϕ – water loss rate constant (in/h or mm/h)
$\phi_{\min}$ – minimum water loss rate constant (in/h or mm/h)
$\phi_{\max}$ – maximum water loss rate constant (in/h or mm/h)
τ – tolerance for the fitting algorithm used to determine ϕ (in or mm)

1. Introduction

Utility-scale solar sites (> 5 MW) are being developed across the state of Virginia, with the potential for more than 350,000 acres being converted to solar by 2045 (McPhillips et al., 2024). Current regulations guiding these projects are based on Virginia House Bill 206, which addresses the potential impacts of small renewable energy projects on natural resources (LIS, 2022). Final regulations associated with HB 206 were published in June 2025. However, there continues to be much uncertainty regarding the extent to which development of utility-scale solar installations alters the magnitude and timing of stormwater delivery. There have been little-to-no measurements of surface runoff from utility-scale solar areas under real-world conditions, and no basis to compare with pre-existing or other land uses. Most solar sites in Virginia are designed using the Virginia Runoff Reduction Method (VRRM), which uses the U.S. Department of Agriculture Natural Resources Conservation Service (NRCS) curve number (CN) approach (U.S. Department of Agriculture, 1986) to generate estimated stormwater runoff quantity and quality. However, it is currently unknown if the assumptions being made and parameters being used when designing utility-scale solar sites are applicable and appropriate.

With funding from the Virginia Department of Environmental Quality (VDEQ), in 2023 we began a six-year study to quantify soil- and stormwater-related impacts of utility-scale solar development. This preliminary report summarizes runoff data collected in Virginia at three utility-scale solar facilities and adjacent reference catchments representing conventional land uses. The three study sites are labeled here as A, B, and C. In this report we outline the methods used for data acquisition and provide early insights into how observed runoff characteristics from monitored rain events can be interpreted using the CN hydrologic method. In addition, we highlight next steps for expanding the monitoring network and data analyses.

2. Methodology

2.1. Rainfall and Runoff Monitoring

Data from this preliminary report are derived from three sites located in the Coastal Plain and Piedmont physiographic provinces of Virginia. Total declared energy capacity at the sites ranged from 17 to 240 MW DC. Solar panels had been installed within the study sites as recently as one year and as long as eight years prior to initiation of monitoring. The sites all had perennial herbaceous cover within the solar arrays and throughout perimeter areas, with some patches of poorly established vegetation, bare soil, and washed-out areas observed at all three sites. Isolated areas within each site required corrective maintenance such as reseeding, regarding, or stabilization during the monitoring period.

We measured rainfall at each site using a weather station with drop-counter rain gauge (ClimaVue 50, Campbell Scientific, Logan, UT, USA) set to record at 5-minute intervals. The rain gauges had a minimum value of 0.1 mm of accumulated precipitation. Rainfall was recorded

starting 1 January 2024 at Site A, 9 September 2024 at Site B, and 19 February 2025 at Site C. Any missing rainfall values were set equal to zero.

At each site, runoff was monitored in three catchments that contained solar arrays and another three catchments outside of developed area as controls. The control sites included a range of land covers, such as agricultural cropland, pastures and lawns, and managed forest stands of different ages. At Site C, delays in receiving permits for soil sampling and installing monitoring equipment meant that we were unable to collect runoff measurements from reference catchments during this initial project period. Runoff was monitored using a 24-in (0.6 m) H-flume that was installed within a stormwater conveyance, e.g., a channel or ditch. All flumes in the solar sites were installed upgradient of stormwater basins (**Figure 1**), and thus are considered to represent direct surface runoff from paneled areas of the sites. Most conveyances were bare soil or vegetated with grass (**Figure 2**), but at Site C one of the ditches was filled with rip-rap and another flume was installed in a rock-lined spillway. Each flume had a conductivity-temperature-depth sensor (TEROS 21, METER Group, Pullman, WA, USA) that was connected to a datalogger (CR350, Campbell Scientific, Logan, UT, USA) and set to record every 5 minutes.

Figure 1*. An H-flume installed in a stormwater conveyance ditch that drains into a permanent stormwater pond in one of the solar sites.*

Figure 2*. An H-flume installed in a drainage ditch in one of the reference catchments.*

Converting measured stormwater flow into an equivalent runoff depth required an accurate estimate of catchment areas. Therefore, we scanned all monitored catchments with a handheld multi-return LiDAR array (Emesent Hovermap ST-X) with a maximum range of 300 m and a resolvable resolution of ± 15 mm. This array employs a Simultaneous Localization and Mapping (SLAM) algorithm, allowing for real-time point cloud processing and greater flexibility in scanning sites with difficult access or limited GPS (Global Positioning System) signal. Satellite images via Google Earth Pro were used to verify or correct acreage in several catchments.

2.2. Catchment Delineation

Point clouds generated by the LiDAR unit were pre-processed and aligned with the manufacturer software (Hovermap Aura), then processed using open-source software (CloudCompare) to remove outliers and separate above-ground artifacts from the ground surface. The output was rasterized into 250 mm voxels, and median height values were exported as GeoTIFF digital elevation models (DEMs). Local DEMs were georeferenced and mosaiced with state-wide data from the Virginia Geographic Information Network (VGIN) to address edge effects. Continuous flow and watershed rasters were derived and converted to polygons at a 250-mm scale.

Some of the sites had high vegetation biomass, standing surface water, or active precipitation while the LiDAR scans were being collected, all of which obscured the ground surface. Those scans proved to be unreliable for accurately delineating catchment boundaries. In some cases, we

were able to use our on-ground observations completed by satellite image analysis to generate reasonable estimates of the catchment areas for purposes of this report. Nonetheless, we will repeat LiDAR scans at those locations when site conditions are appropriate.

2.3. Storm Delineation

We used an automated procedure to define and compare storm events: a rainfall event was considered to begin when measurable rainfall was observed (i.e., > 0.1 mm per 5-minute interval) and then ended once a minimum dry period of six hours had passed without additional rainfall. The inter-event time criterion was used so that closely spaced precipitation events were not grouped into a single event. However, two sets of events, one in Site B and one in Site C, were so closely spaced that surface runoff from the first event was still occurring when the second event started. Therefore, we manually merged the two events in both instances.

Storms with a total rainfall depth of at least 4 mm were initially retained for further analysis, as smaller events typically produced negligible or no runoff. Note that this criterion was less than that used for development of erosion models such as the Universal Soil Loss Equation (USLE) and its revisions (i.e., RUSLE and RUSLE2), which have a minimum storm threshold of 12.7 mm when calculating rainfall erosivity factors (Yin et al., 2017). For each identified event, the start and end times, duration, and total accumulated rainfall were calculated.

Rainfall rates were converted to hourly intensities by multiplying the amount of rainfall accumulated in five minutes by 12 (thus converting from per minutes to per hours). Peak 15-minute rainfall intensity was calculated for each storm by averaging rainfall intensity across three consecutive 5-minute bins.

2.4. Runoff Quantification

Measurements of water stage, h (in ft), were converted to volumetric discharge, q (in cfs), using the following rating curve (Walkowiak, 2006):

$$q = 2.23h^{2.31} \quad (1)$$

A comparison of this rating curve versus the one provided by the United States Geological Survey (Kennedy, 1984) is presented in **Appendix A**.

Calculated q values were then converted into cubic meters per second (m^3/s). Any missing flow values were linearly interpolated from observations before and after the gap.

We performed a flow correction procedure to mitigate potential sensor drift and account for any perennial or intermittent flow in the drainages. The corrected flow, $q_{adjusted}$, was derived by subtracting the minimum flow measured during each storm event ($q_{minimum}$) from the flow measured during each time step of the event:

$$q_{adjusted} = \max(q - q_{minimum}, 0) \quad (2).$$

Our procedure also required estimates for the time of the start (t_{q0}) and end (t_{qe}) of the runoff event. To identify the start of the runoff event, we set a threshold flow value ($q_{threshold}$) that was the greater of 5% above the minimum value of $q_{corrected}$ or 0.2 cfm. We then identified t_{q0} as the first time after $q_{threshold}$ was met in which the first derivative of the hydrograph was greater than 1 x 10^{-4} cfm/s (i.e., $dq/dt > 1 \times 10^{-4}$ cfm/s) for three consecutive 5-minute intervals. To identify the end of the runoff event, t_{qe}, we first identified the time of peak discharge (t_{pk}), then searched forward in time for the first instance of at least three consecutive 5-minute samples in which (i) discharge had fallen below the greater of $q_{threshold}$ or 1% of the event peak, and (ii) the hydrograph slope was greater than -1×10^{-4} cfm/s (i.e., $dq/dt > -1\times10^{-4}$ cfm/s) for three consecutive 5-minute intervals. If the above two conditions were not met, then the runoff event was considered to have ended after 12 hours past the end of rainfall or the beginning of the next storm event, whichever came sooner.

Runoff intensity, q_{depth} (in mm/h), was calculated by normalizing stormflow by catchment area:

$$q_{depth} = \frac{q_{stormflow}}{A} \times 1000 \times 3600 \quad (3)$$

where $q_{stormflow}$ is the corrected stormflow in m^3/s and A is the contributing area in m^2.

Runoff volume (in m^3) was determined by integrating $q_{stormflow}$ over the storm event window ($t_{q0} \leq t < t_{qe}$):

$$V_{runoff} = \sum_{i=t_{q0}}^{t_{qe}} q_{stormflow}(t_{i+1} - t_i) \quad (4)$$

Runoff depth, Q (mm), was obtained by dividing the runoff volume (m^3) by catchment area (m^2) and converting to mm:

$$Q = \frac{V_{runoff}}{A} \times 1000 \quad (5)$$

Finally, the rainfall–runoff ratio, R, was calculated as:

$$R = \frac{Q}{P} \quad (6)$$

where P is the total accumulated rainfall in mm.

2.5. Time of Concentration Analysis

We quantified the time of concentration for each catchment, using a definition based on centroids of effective precipitation and runoff (McCuen, 2009):

$$T_c = t_{pc} - t_{qc} \quad (7)$$

where t_{pc} is the time associated with the centroid of the effective precipitation input and t_{qc} is the time associated with the centroid of the surface runoff response. We quantified these metrics on a

subset of storms in Site A, focusing on a set of three storms that produced surface runoff in all catchments. The storms occurred on 27 September 2024, 17 March 2025, and 21 May 2025.

Because precipitation data recorded by the weather stations is in gross rainfall (P, in mm per interval), the first step of this analysis was to quantify the effective precipitation, P^*, which represents the amount of rainfall that became translated to surface runoff. By definition:

$$P^* = Q \tag{8}$$

We derived P^* using a ϕ-index approach that included an estimate of the initial abstraction, I_a (Chow et al., 1988; Bedient et al., 2019; U.S. Department of Agriculture, 1986), where ϕ represents a constant loss rate (U.S. Army Corps of Engineers, 2023). We quantified I_a as the cumulative amount of precipitation that had fallen prior to the start of direct runoff (i.e., t_{q0}). We then used a fitting algorithm to identify the ϕ value that best met the condition of Eq. 7, as described in **Appendix B**. Once ϕ was determined we calculated the effective precipitation for each time step, p_i^*.

We next calculated t_{pc} as the weighted mean of mid-interval times using effective rainfall as weights:

$$t_{pc} = \frac{\sum_i p_i^* t_{mid,i}}{\sum_i p_i^*} \tag{9}$$

where $t_{mid,i}$ is the midpoint time of interval i, expressed as hours since event start.

Similarly, we calculated t_{qc} as the weighted mean of the hydrograph over the detected runoff window as:

$$t_{qc} = \frac{\sum_i q_{adjusted,i}\, t_{mid,i}}{\sum_i q_{adjusted,i}} \tag{10}.$$

2.6. Curve Number Analysis

We analyzed event rainfall–runoff pairs (P and Q; depths in inches) to determine the best-fit CN for each monitored catchment. The CN formulation estimates Q as:

$$Q(P; CN; \lambda) = 0,\ for\ P \le \lambda\, S \tag{11a}$$

$$Q(P; CN; \lambda) = (P - \lambda\, S)^2/(P + (1 - \lambda)\, S), for\ P > \lambda\, S \tag{11b}$$

$$S = \frac{1000}{\mathrm{CN}} - 10 \tag{11c}$$

where S is the storage in the catchment after runoff begins and λ is the initial abstraction ratio, i.e., $\lambda = I_a/S$. It is often assumed that $\lambda = 0.20$ (Chin, 2017; Auerswald & Gu, 2021), but others have argued that $\lambda = 0.05$ is more appropriate. For our analysis we estimated best-fit CNs using an automated least-squares algorithm, with the CN model fit to observed P and Q values for each

catchment. We constrained the analysis to storms with R values greater than or equal to the median (i.e., the top 50% of storms by relative amounts of runoff), so as to better characterize runoff potentials. We performed two fits per catchment, assuming that 1) $\lambda = 0.20$ or 2) $\lambda = 0.05$.

3. Results

3.1. Catchment Delineations

The catchments ranged in size from 1.4 to 6.4 ha (3.4 to 15.8 acres; **Table 1**).

***Table 1**. Catchment areas as delineated by our handheld LiDAR array with SLAM mapping. Catchment areas are presented in hectares (ha) with the equivalent area in acres in parentheses.*

Site	Catchment Type	Area in ha (acres)
A	Solar Panels (#1)	2.5 (6.3)
A	Solar Panels (#2)	2.8 (7.0)*
A	Solar Panels (#3)	1.6 (4.0)*
A	Corn-Soybean Crop Field	4.6 (11.3)*
A	Grass-Forest Mixture	3.2 (8.0)
B	Solar Panels (#1)	3.7 (9.2)
B	Solar Panels (#2)	4.1 (10.1)
B	Soybean Crop Field	6.4 (15.8)
C	Solar Panels (#1)	2.3 (5.6)
C	Solar Panels (#2)	3.3 (8.2)
C	Solar Panels (#3)	1.4 (3.4)

*Catchment area delineation created or modified using Google Earth.

3.2. Storm Events

In total, 76 storms were detected by the weather station at Site A between 1 January 2024 and 1 October 2025. Site B had 39 recorded storms between 15 September 2024 and 1 October 2025. Site C received 41 storms between 19 February 2025 and 1 October 2025. The majority of storms had < 25 mm of accumulation, with storms < 10 mm being the most common (**Figure 3**).

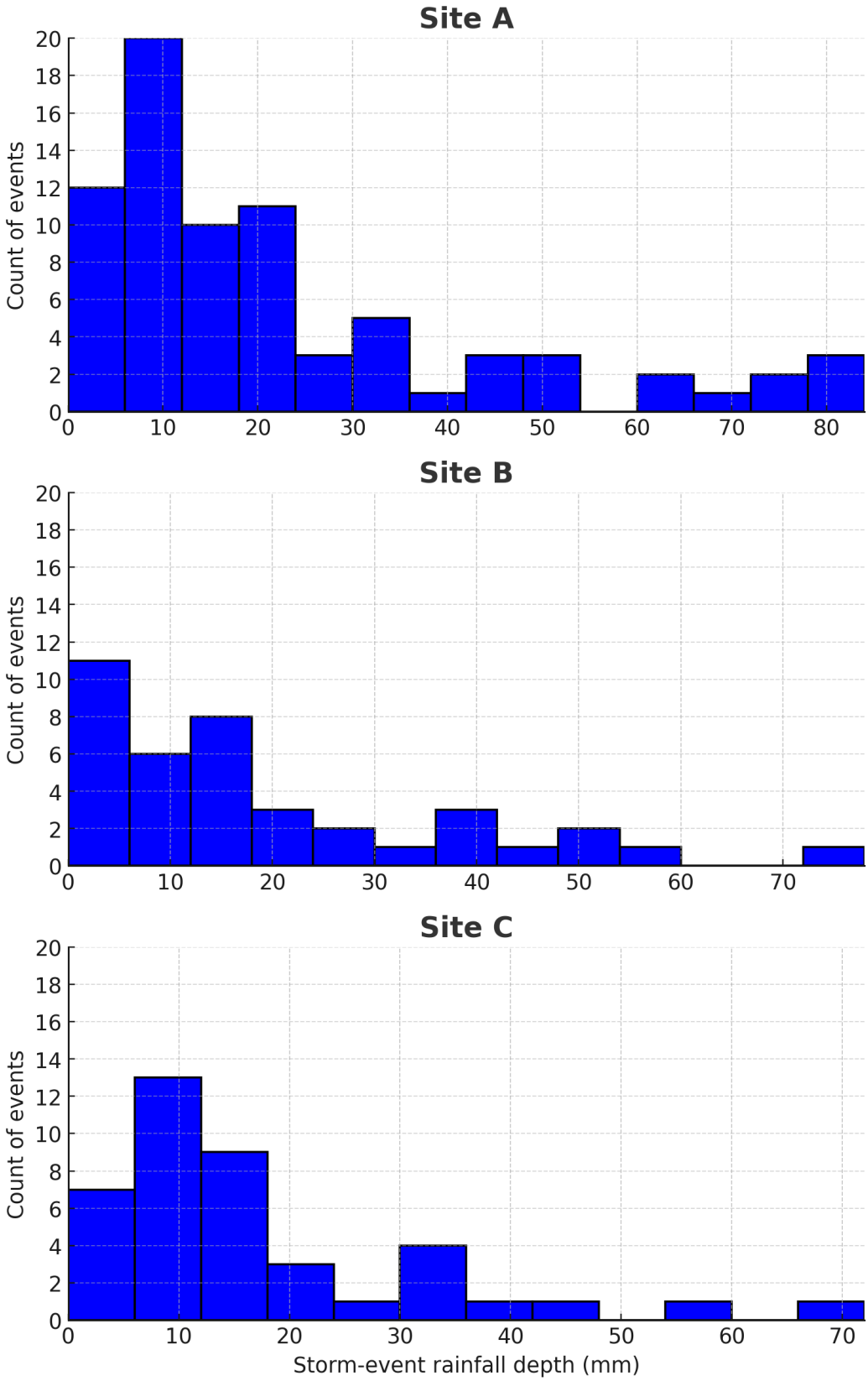

Figure 3. *Distributions of rainfall depth (mm) recorded at three monitoring sites (A, B, and C).*

It is important to note that, based on these first 1-2 years of data collection, none of the monitored storms exceeded the locally defined 10-year, 24-hour rainfall depth. The 10-year, 24-hr benchmark is 137 mm (~5.4 inches) at Site A, 125 mm (~4.9 inches) at Site B, and 125 mm (~4.9 inches) at Site C, while the largest storms observed at the sites were 82 mm (~3.2 inches) at Site A, 76 mm (~3.0 inches) at Site B, and 69 mm (~2.70 inches) at Site C. These events were similar in magnitude to 1- to 2-year events (**Table 2**). The results presented here should therefore be considered to reflect common storm conditions rather than relatively rare, intense rainfall events. Future updates will be needed as we capture more and larger storm events.

Table 2*. The largest observed storm at each study site (Sites A, B, and C) compared to design storm depths based on expected return periods of 1-, 2-, 5-, and 10 years. Design storm values were obtained for 24-h periods from NOAA Atlas 14 precipitation frequency estimates, while observed depths represent the maximum storm depth recorded over any 24-h period in the study.*

Site	Largest observed storm	1-yr return period	2-yr return period	5-yr return period	10-yr return period
	---------- 24-h storm depth in mm (inches) ----------				
A	81.7 (3.22)	73.4 (2.89)	89.4 (3.52)	115.3 (4.54)	137.4 (5.41)
B	75.7 (2.98)	68.1 (2.68)	82.6 (3.25)	105.4 (4.15)	124.7 (4.904)
C	68.9 (2.71)	68.3 (2.69)	82.8 (3.26)	105.9 (4.17)	125.2 (4.93)

3.3. Hyetograph and Hydrograph Examples

Rainfall hyetographs and runoff hydrographs are presented for three storms, ranging from 27 to 76 mm, as measured at Site A (**Figure 4**), Site B (**Figure 5**), and Site C (**Figure 6**). These hydrographs are useful for comparing the timing and magnitude of surface runoff during and after precipitation. They also indicate the variability in surface runoff responses between catchments, and also within the same catchments for different storms with different antecedent conditions. The catchments with solar panel arrays tended to respond quickly to storm events, whereas the reference catchments tended to only produce appreciable surface runoff once sufficient precipitation had accumulated. In Site A, the corn-soybean field produced greater peak runoff amounts than the solar catchments during certain storms (e.g., **Figure 4a** and **4c**). Nonetheless, the corn-soybean field tended to produced less or similar amounts of total runoff compared to the solar catchments during these storms.

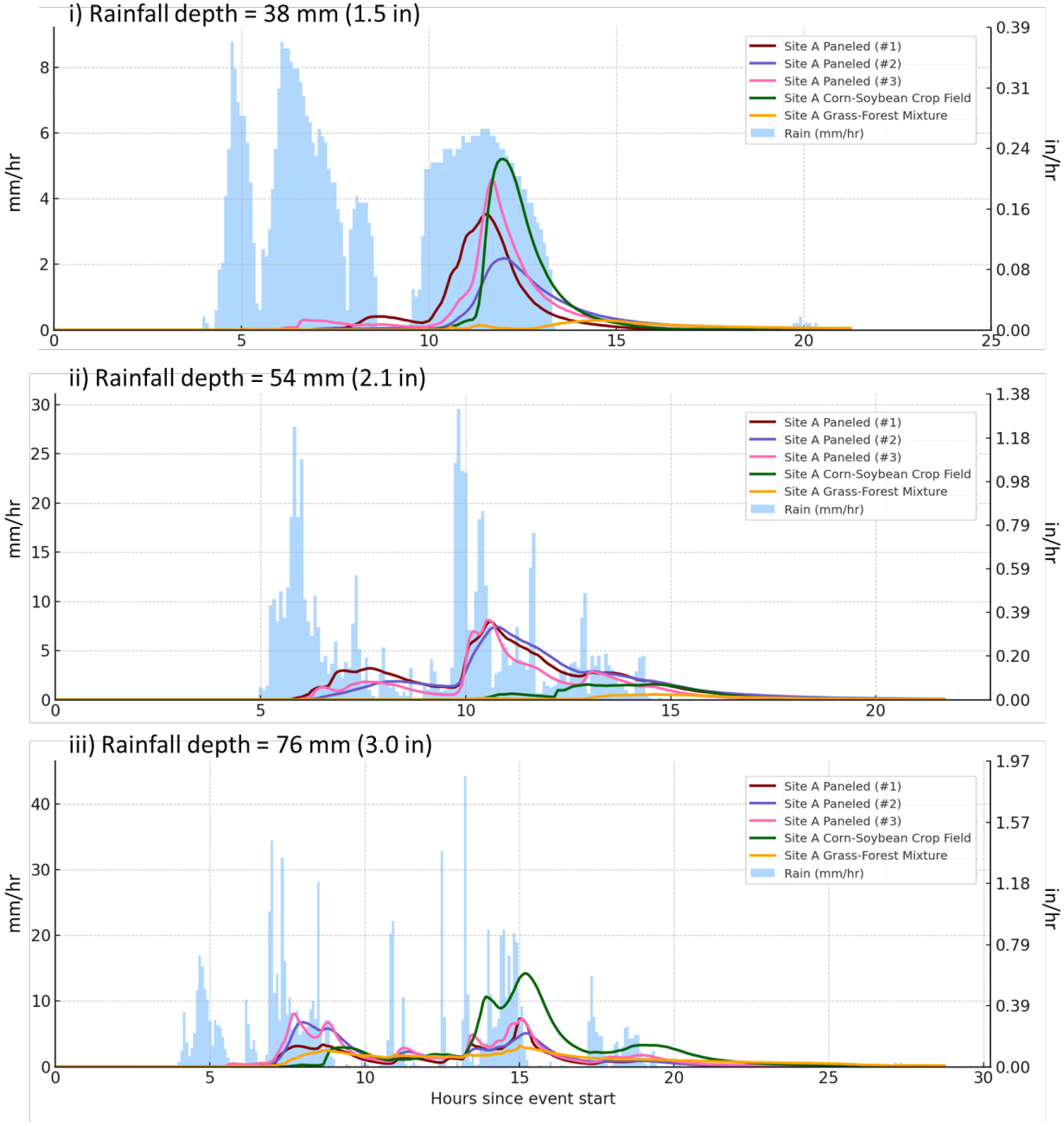

Figure 4. *Rainfall hyetographs (blue bars) and runoff hydrographs (solid lines) as measured in four catchments at Site A during three storms: i) a 38-mm rain event on 31 January 2025; ii) a 54-mm event on 11 December 2024, and iii) a 76-mm event on 16 March 2025. Note that the axis scales vary between graphs.*

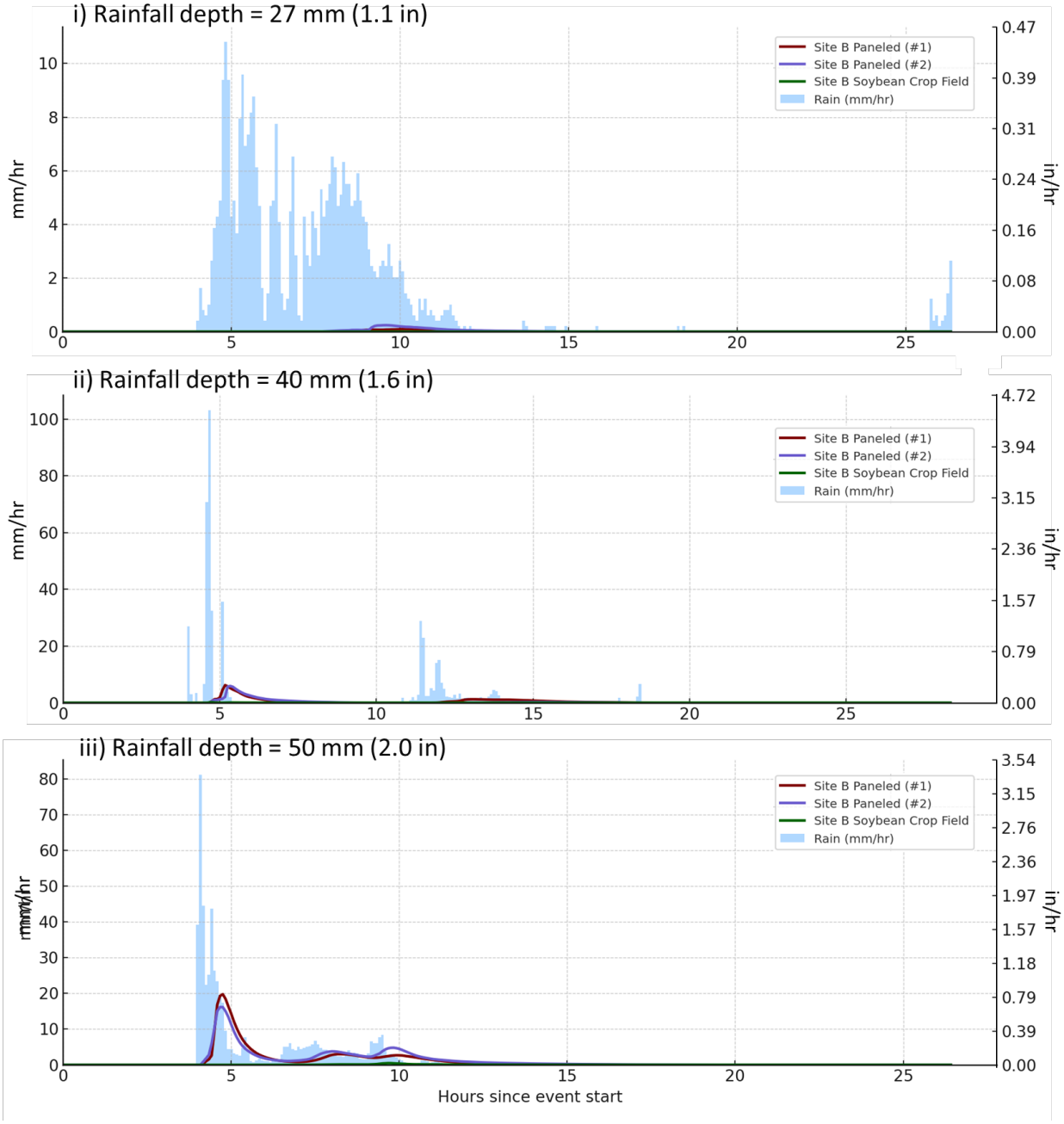

Figure 5. *Rainfall hyetographs (blue bars) and runoff hydrographs (solid lines) as measured in two catchments at Site B during three storms: i) a 27-mm rain event on 29 August 2025; ii) a 40-mm event on 1 June 2025, and iii) a 50-mm event on 9 July 2025. Note that the axis scales vary between graphs.*

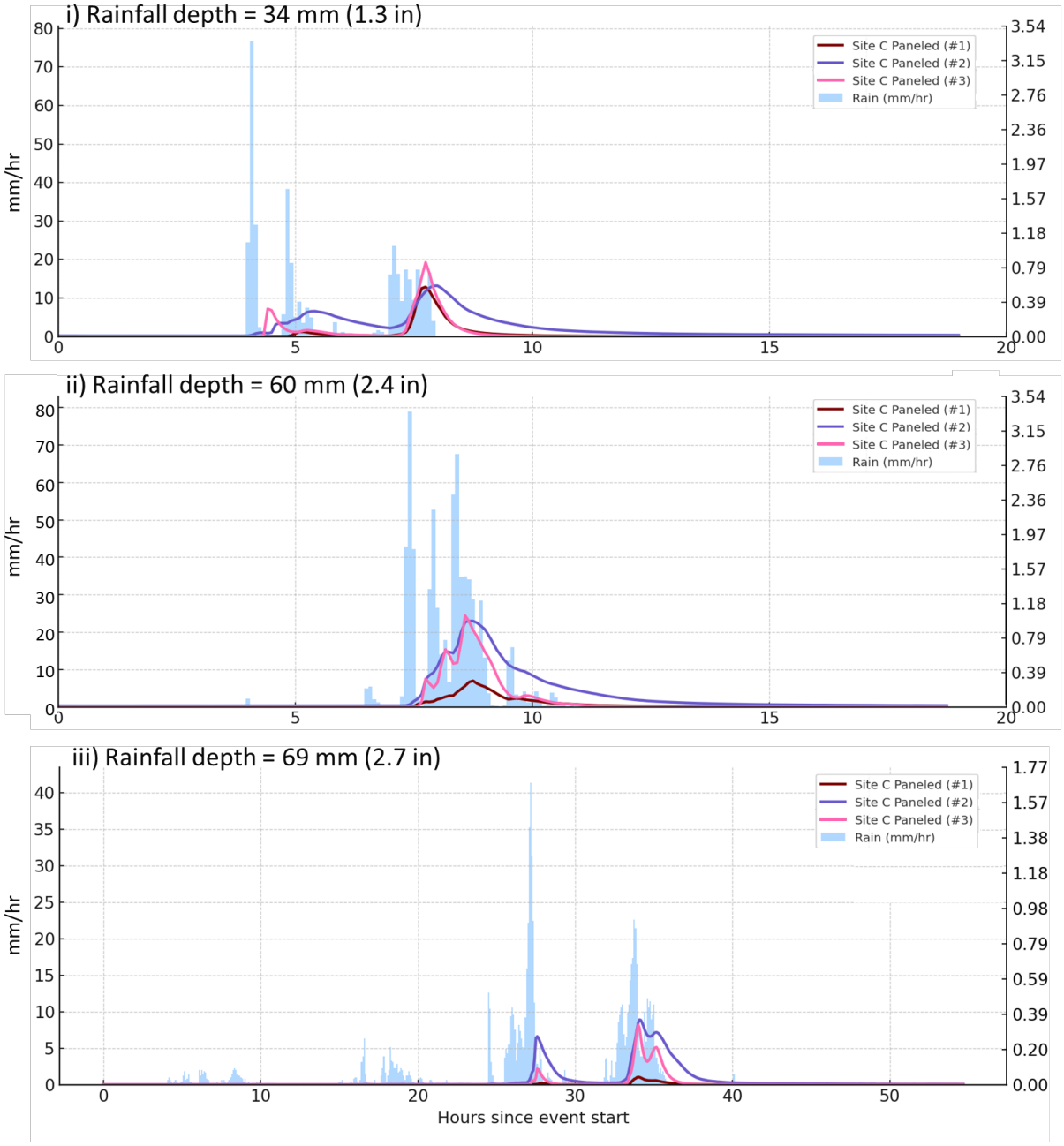

Figure 6. *Rainfall hyetographs (blue bars) and runoff hydrographs (solid lines) as measured in three catchments at Site C during three storms: i) a 34-mm rain event on 12 July 2025; ii) a 60-mm event on 8 July 2025, and iii) a 69-mm event on 16 September 2025. Note that the axis scales vary between graphs.*

3.4. Rainfall-Runoff Statistics

We compiled rainfall and runoff statistics for selected catchments in our three study sites (**Table 3**), based on recorded storms with ≥ 25 mm of accumulation and available runoff data for each catchment. There were up to 20 such storms in Site A, up to 11 storms in Site B, and up to 8 storms in Site C. Median *Q* values were larger in paneled catchments compared to corresponding reference catchments, regardless of whether the storms were ordered by total runoff amount (*Q*) or relative runoff amount (*R*). For example, at Site A the median storm (by *Q*) produced *R* values of 0.10-0.20 in the catchments with solar development (meaning that 10-20% of *P* was converted into measurable *Q*), versus 0.02 in the two reference catchments. The differences were greater when storms were sorted by *R*: paneled catchments had median *R* values of 0.13-0.30, versus 0.02 in the reference catchments. The two paneled catchments at Site B had median *R* ratios of 0.15 and 0.66 versus 0.03 in the reference crop field. Median R values varied from 0.04 to 0.95 in Site C. When sorted by *Q*, maximum *R* ratios ranged from 0.41 to 0.99 in catchments with solar development, whereas the three analyzed reference catchments ranged from 0.20 to 0.47. When sorted by *R*, maximum *R* values were 0.59 – 0.99 in catchments with solar arrays.

Table 3*. Summary of runoff metrics for monitored catchments, based on all storm events with ≥ 25 mm of total accumulated precipitation (P). The median and maximum runoff amounts are presented for each catchment, with runoff ordered both by the total depth of accumulated runoff (Q) and by the runoff ratio (R = Q/P). Each column presents the runoff depth in mm and the corresponding runoff ratio in parentheses.*

Site	Catchment	Number of events	Median runoff		Maximum runoff	
			By *Q*	By *R*	By *Q*	By *R*
A	Paneled 1	20	11.4 (0.15)	24.3 (0.30)	39.2 (0.48)	20.1 (0.65)
A	Paneled 2	18	6.8 (0.20)	6.8 (0.20)	32.0 (0.49)	20.7 (0.67)
A	Paneled 3	17	6.4 (0.10)	10.4 (0.13)	31.1 (0.41)	29.5 (0.96)
A	Corn-Soybean	19	0.5 (0.02)	0.5 (0.02)	35.4 (0.47)	24.6 (0.80)
A	Grass/Forest	17	0.8 (0.02)	0.8 (0.02)	16.5 (0.22)	7.2 (0.23)
B	Paneled 1	11	16.8 (0.66)	15.0 (0.31)	55.8 (0.99)	55.8 (0.99)
B	Paneled 2	3	6.2 (0.15)	6.2 (0.15)	29.4 (0.59)	29.4 (0.59)
B	Soybean	7	1.0 (0.03)	1.1 (0.02)	11.3 (0.20)	11.3 (0.20)
C	Paneled 1	8	2.5 (0.04)	2.5 (0.04)	14.4 (0.16)	10.6 (0.31)
C	Paneled 2	8	24.1 (0.95)	32.9 (0.50)	81.0 (0.88)	34.0 (0.99)
C	Paneled 3	8	5.6 (0.22)	12.4 (0.18)	33.3 (0.36)	33.3 (0.36)

3.5. Time of Concentration

An example set of runoff responses and timing metrics, including T_c, are shown in **Appendix C** for a storm that occurred on 27 September 2024 and had 50.1 mm of total precipitation. That storm translated to P^* values from 21 to 30 mm in the solar catchments (**Figures C1-C3**), 22 mm in the catchment with the corn-soybean field (**Figure C4**), and only 3.3 mm in the grass-forest catchment (**Figure C5**). Calculated I_a was around 7 mm for two of the three catchments with solar panels and the corn-soybean field. The ϕ loss rate was also similar between the solar catchments and the corn soybean field, ranging from 6.7 to 15 mm/h. The grass-forest catchment had much greater storage, with I_a = 30 mm and ϕ = 38 mm/h, and as a consequence had much less Q. Calculated T_c values for that storm were 0.8 to 1.8 h in the solar catchments, 0.2 h in the catchment with the corn-soybean field, and 2.9 h in the catchment with the grass and forest areas.

The T_c values compiled from the other two storms (16 March and 21 May) tended to be longer for the various catchments, likely due in part to the precipitation being spread out over a longer period (**Table 4**). Mean T_c values in the solar catchments varied from 1.2 to 2.1 h, similar to the 1.7 h found in the corn-soybean catchment. The T_c for the grass-forest catchment was greater for every storm, indicating a slower hydrological response.

Table 4*. Calculated time of concentration (T_c) values for three storms analyzed at different catchments at Site A.*

Site	Catchment Type	Storm 1 (2024-09-07)	Storm 2 (2025-03-16)	Storm 3 (2025-05-21)	Mean (± SD)
		T_c (h)			
A	Paneled 1	0.9	2.3	0.9	1.4 ± 0.8
A	Paneled 2	1.8	1.2	3.3	2.1 ± 1.1
A	Paneled 3	0.8	1.6	2.4	1.6 ± 1.2
A	Corn-Soybean	0.2	2.7	2.1	1.7 ± 1.3
A	Grass/Forest	2.9	3.8	3.7	3.5 ± 0.5

3.6. Curve Number Analysis

The observed values of *P* and *Q* corresponded to a wide range of CN values for each monitored catchment at Site A (**Figures 7-11**). For example, the catchments monitored in the paneled areas had many storms whose measured *P*-*Q* values translated to apparent CN values > 80. Other storms had little-to-no measurable *Q*. The reference catchments also had some storms with CN > 80, but relatively fewer above this level than the catchments with solar panels. When compiled across the top 50% of storms (by relative runoff amounts), the best-fit CNs ranged from 76.8 to 84.3 in the paneled catchments, whereas the reference catchment with a corn-soybean field had a best-fit CN of 75.5. The grass-forest catchment had a much lower best-fit CN of 61.8.

In Site B, the best-fit CNs also varied between the catchments within the solar arrays versus the local reference catchment. The paneled catchments had relatively large CN values, with the best-fit CN = 90.7 in one catchment (**Figure 12**) and CN = 87.6 in the other (**Figure 13**). The reference catchment, which primarily contained a soybean field, had a best-fit CN of 67.5 (**Figure 14**). However, it is worth noting that the number of recorded storms were limited in the second solar catchment and the soybean field catchment. It is therefore likely that these best-fit CN values have some uncertainty, but it is still notable that individual storms had consistently greater *Q* values in the solar catchment compared to the reference.

As shown in **Appendix D**, the catchments with solar panels in Site C had a wide range of apparent CNs, with CN = 59.5 for the first catchment (**Figure D1**), CN = 94.5 for the second (**Figure D2**), and CN = 73.7 for the third (**Figure D3**). However, several caveats apply to these results. As was the case in Site B, the best-fit CNs in Site C were generated based on a limited number of storms (each curve was fit to only four storms), and therefore are also likely to have considerable uncertainty. Moreover, the flume in the first catchment was placed in a rock-lined spillway that may have allowed some runoff to bypass the flume, leading to possible under-estimations. We expect to revisit the site soon and verify the flume performance then. Finally, we are not able to provide a comparison with reference catchments yet at this site, but we anticipate having sufficient data to do so with another year of monitoring.

Under the assumption of a smaller initial abstraction value (i.e., $\lambda = 0.05$), all of the best-fit CN values decreased to some extent (as shown in **Appendix E**). At Site A, the catchments with solar arrays had best-fit CNs that ranged from 67.4 to 78.7 (**Figures E1-E3**), slightly greater than the best-fit CN of 66.0 determined in the corn-soybean catchment (**Figure E4**). The grass-forest catchment at Site A had a best-fit CN of 44.9 (**Figure E5**), near the lower limit of possible CN values (i.e., CN > 30). The catchments with solar panels at Site B continued to have relatively large CN values, with the best-fit CN = 87.9 for one catchment (**Figure E6**) and CN = 83.6 for the other (**Figure E7**). The catchment containing the soybean field there had a best-fit CN = 48.5 (**Figure E8**). Best-fit CNs ranged from 46.4 to 92.9 for the three catchments with solar arrays at Site C (**Figures E9-E11**).

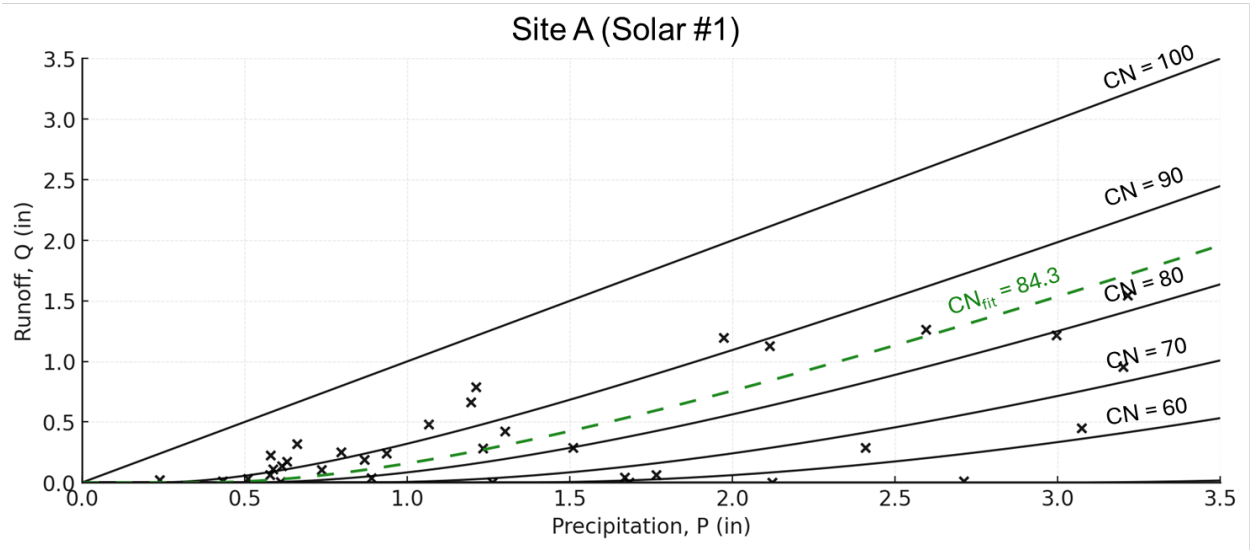

***Figure 7**. Precipitation (P) and runoff (Q) for different storms measured at Site A in a catchment developed with solar panels (points), along with the P-Q relationships modeled by different curve number (CN) values assuming initial abstraction λ = 0.20 (solid lines). The dashed green line indicates the CN value that best fits the top 50% of storms (by relative runoff) using least-squares regression.*

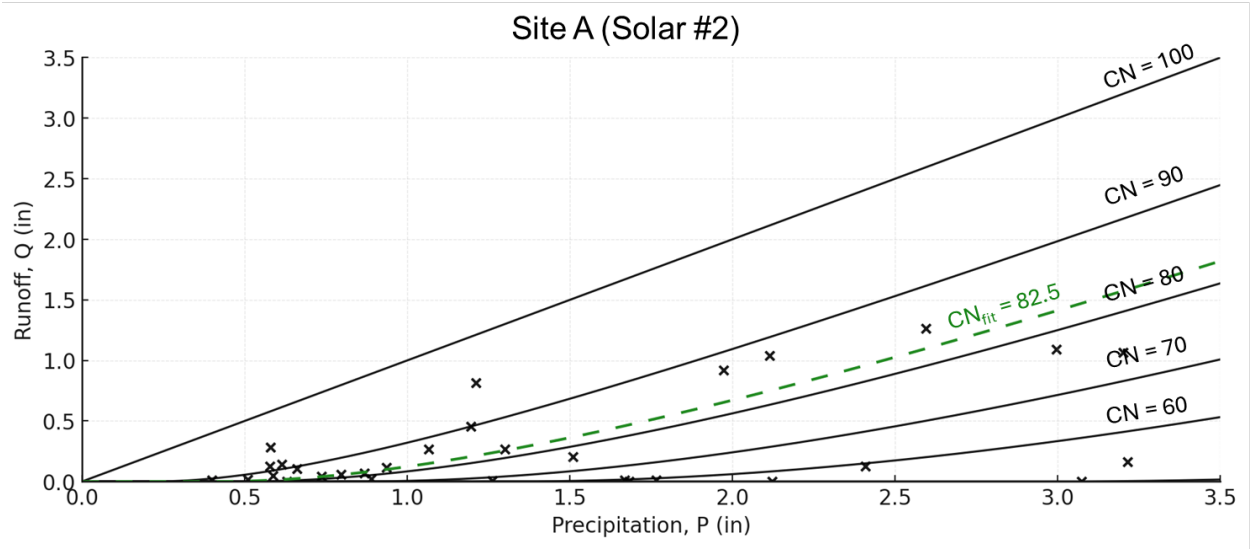

***Figure 8**. Precipitation (P) and runoff (Q) for different storms measured at Site A in a catchment developed with solar panels (points), along with the P-Q relationships modeled by different curve number (CN) values assuming initial abstraction λ = 0.20 (solid lines). The dashed green line indicates the CN value that best fits the top 50% of storms (by relative runoff) using least-squares regression.*

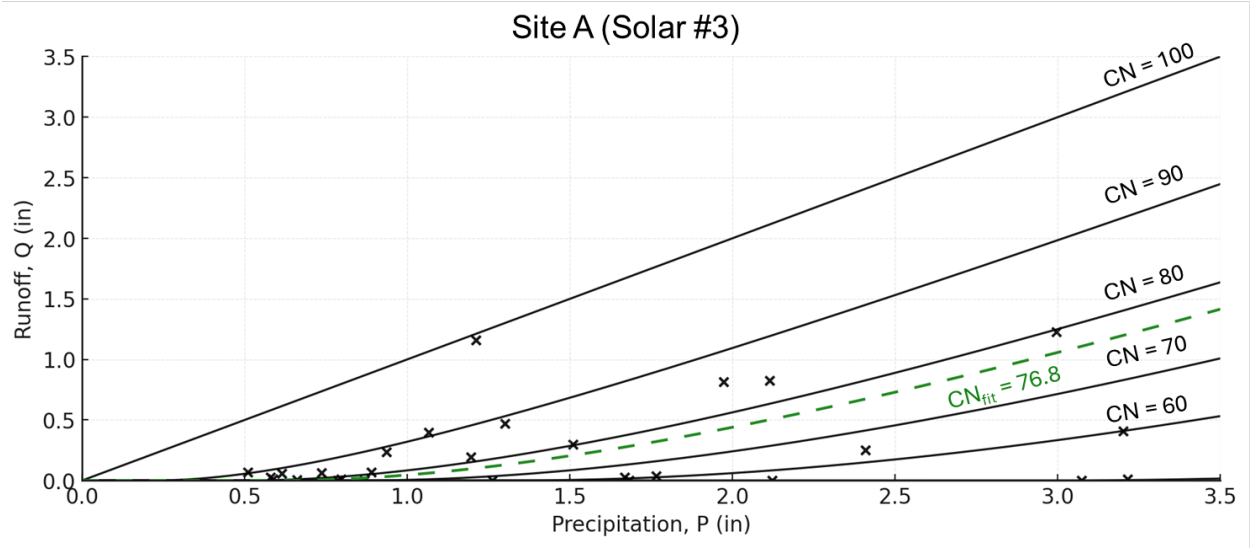

Figure 9. *Precipitation (P) and runoff (Q) for different storms measured at Site A in a catchment developed with solar panels (points), along with the P-Q relationships modeled by different curve number (CN) values assuming initial abstraction λ = 0.20 (solid lines). The dashed green line indicates the CN value that best fits the top 50% of storms (by relative runoff) using least-squares regression.*

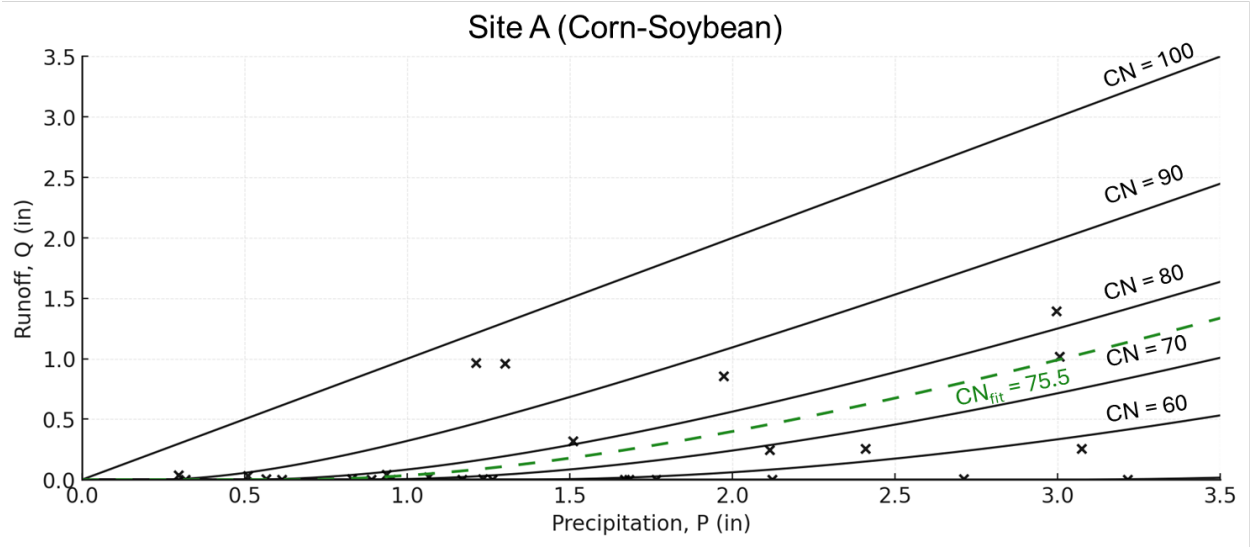

Figure 10. *Precipitation (P) and runoff (Q) for different storms measured at Site A in a reference catchment planted in a corn-soybean rotation (points), along with the P-Q relationships modeled by different curve number (CN) values assuming initial abstraction λ = 0.20 (solid lines). The dashed green line indicates the CN value that best fits the top 50% of storms (by relative runoff) using least-squares regression.*

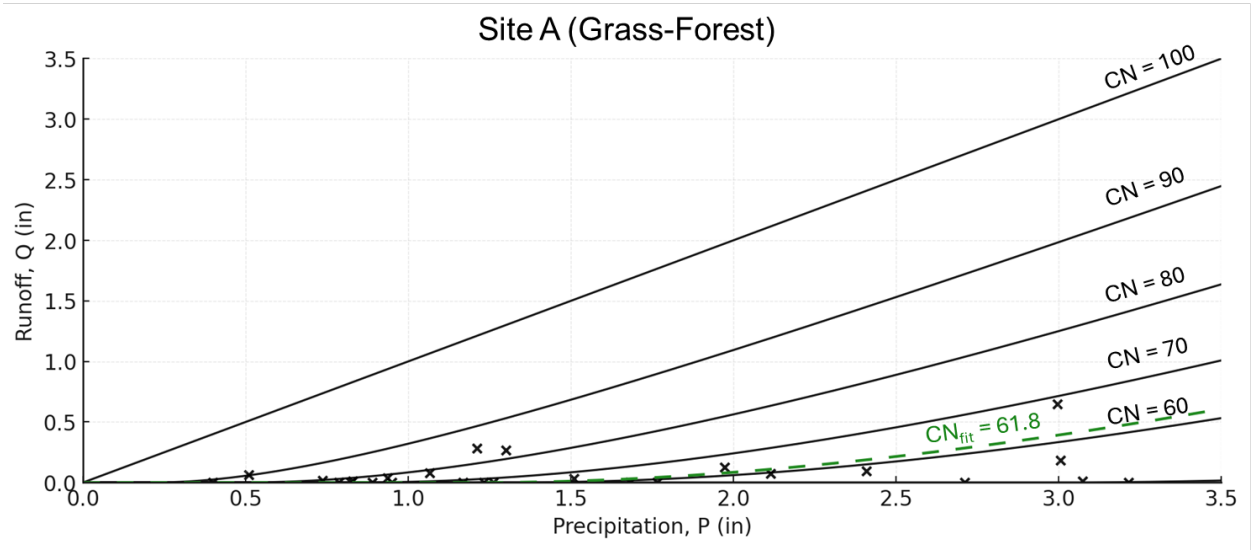

Figure 11. *Precipitation (P) and runoff (Q) for different storms measured at Site A in a reference catchment with mixed grassed and forested areas (points), along with the P-Q relationships modeled by different curve number (CN) values assuming initial abstraction λ = 0.20 (solid lines). The dashed green line indicates the CN value that best fits the top 50% of storms (by relative runoff) using least-squares regression.*

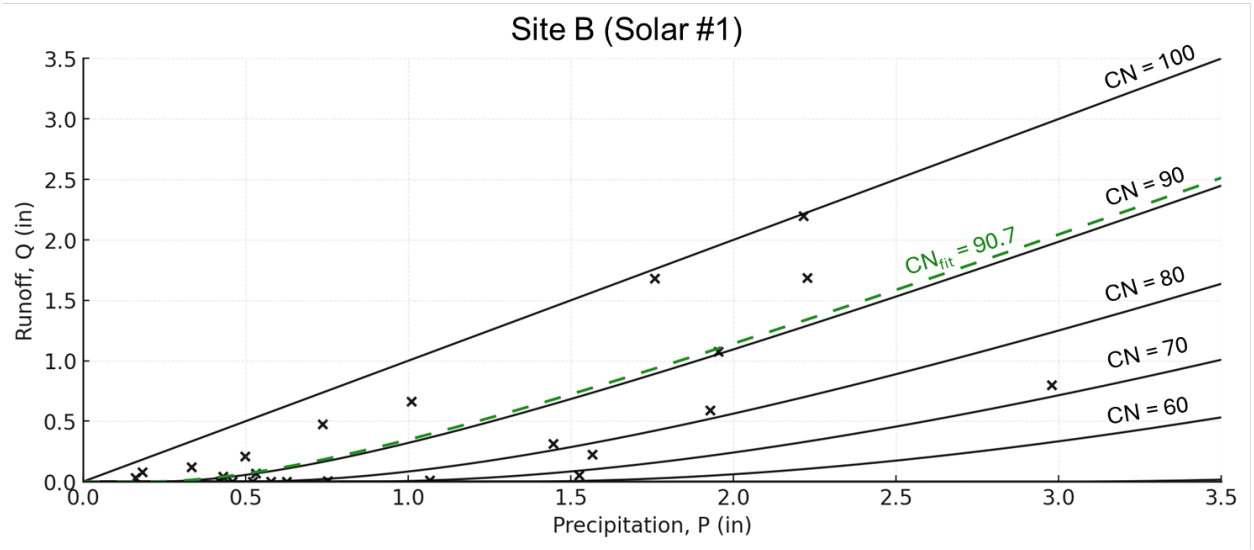

Figure 12. *Precipitation (P) and runoff (Q) for different storms measured at Site B in a catchment developed with solar panels (points), along with the P-Q relationships modeled by different curve number (CN) values assuming initial abstraction λ = 0.20 (solid lines). The dashed green line indicates the CN value that best fits the top 50% of storms (by relative runoff) using least-squares regression.*

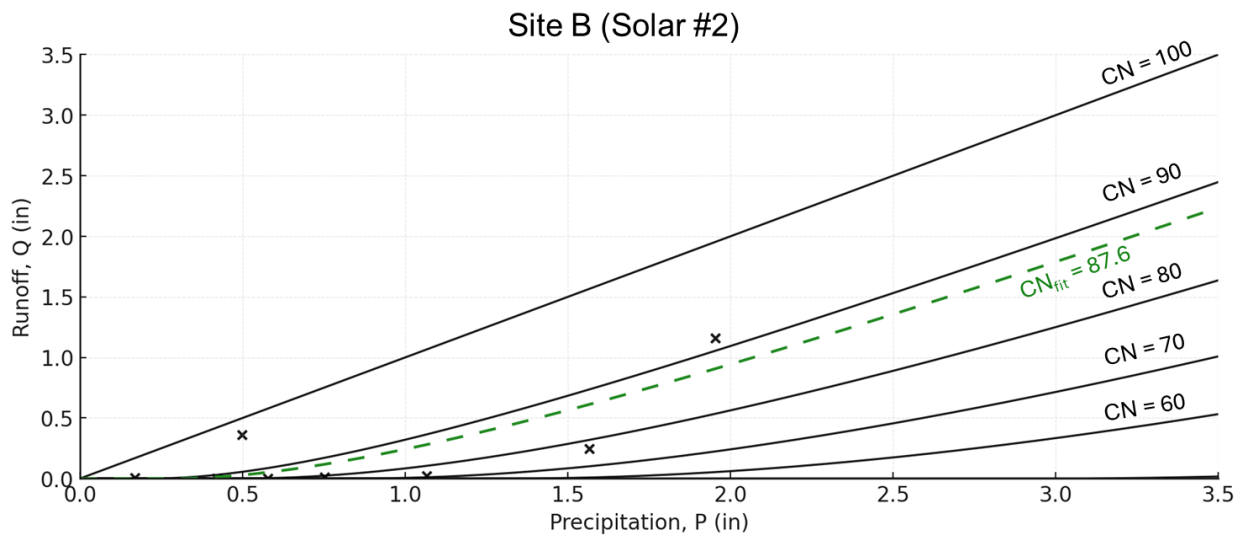

Figure 13. *Precipitation (P) and runoff (Q) for different storms measured at Site B in a catchment developed with solar panels (points), along with the P-Q relationships modeled by different curve number (CN) values assuming initial abstraction λ = 0.20 (solid lines). The dashed green line indicates the CN value that best fits the top 50% of storms (by relative runoff) using least-squares regression.*

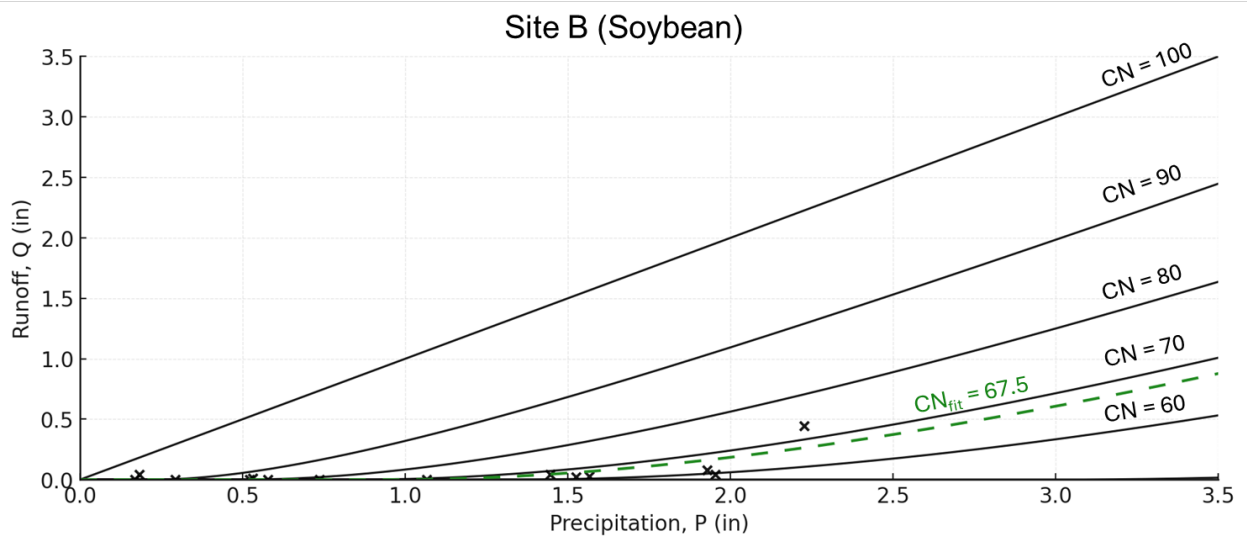

Figure 14. *Precipitation (P) and runoff (Q) for different storms measured at Site B in a catchment with a soybean field (points), along with the P-Q relationships modeled by different curve number (CN) values assuming initial abstraction λ = 0.20 (solid lines). The dashed green line indicates the CN value that best fits the top 50% of storms (by relative runoff) using least-squares regression.*

4. Interpretation and Next Steps

Our preliminary data and analyses showed that catchments within solar arrays tended to produce rapid, and at times substantial, amounts of surface runoff during storms. Paneled catchments had greater median *R* ratios compared to the reference catchments, indicating less stormwater retention within the landscape. Many individual storms translated to apparent CN values > 80 for solar areas, though other storms, including several events with > 2 in of accumulated *P*, did not produce appreciable *Q*. The reference catchments also had considerable variability in the relative amount of *Q* produced during different storms. While the number of reference catchments included in this analysis is limited compared to what will be contained within the full dataset, they do indicate hydrologic differences compared to catchments that contain solar arrays, including lesser amounts of surface runoff for many storms and shorter times of concentration. In particularly, the catchment at Site A characterized by perennial grass and forested areas had substantially less surface runoff volumes with greater times of concentration.

Best-fit CNs, which were determined using a least-square regression fitting to the top 50% of storms (by relative runoff), varied between individual catchments and sites. The best-fit CN numbers exceeded 74 in all but one of the catchments with solar panels (n = 8), with all but three catchments having CN values > 80 and two of the catchments with CN values > 90. In comparison, the reference catchments had best-fit CNs that ranged from 61.8 (an area with forests and grass) to 75.5 (an area with a row crop field). These results imply that the solar development is resulting in greater runoff volumes for the typical type of storm that occurs in these areas. We speculate that one reason for this increased stormwater is changes in soil hydraulic properties, such as reduced permeability, increased bulk density, and decreased internal drainage of the soils (Hyland, 2025). Another reason could be changes in the types and rooting depths of vegetation at these sites, although two of the three reference catchments were primarily characterized by row crop production. Using a combination of in-field and laboratory measurements, we are characterizing soil properties – including texture, bulk density, and saturated hydraulic conductivity – along transects established in each catchment. We intend to use these observations to inform if and how solar development alters soil properties. Those same transect points are also being used for vegetation surveys, which will allow us to better evaluate how factors such as vegetation type and density influence runoff lag times from solar sites.

The choice of λ value continues to be a point of debate when using the curve number approach. A recent recommendation was to use $\lambda = 0.20$ in the eastern U.S. as a more conservative design choice (Moglen et al., 2025). Our analysis supports this recommendation, as the best-fit CNs were larger when assuming $\lambda = 0.20$ rather than 0.05. We also anticipate that, with continued data collection, we will be able to provide recommendations to estimate CNs based on either value of λ. There is also the possibility of using the observed data to recommend λ values that vary with the amount of storage available, such that λ can be estimated as a function of the CN used in the design (Chin, 2017).

These preliminary results also emphasize that storm timing and intensity are important factors in the amount of runoff generated from these catchments: consistent storms with low rainfall intensity tended to produce less runoff than storms of similar magnitude with greater rainfall intensity over shorter times. The CN approach only accounts for such dynamics based on the storm distribution type, which causes the theoretical CN value to shift for a given infiltration capacity (Chin, 2017). Current NRCS guidance divides 24-hour storms into four distribution types (I, IA, II, and III), with most of Virginia considered Type II (U.S. Department of Agriculture, 2021). As seen in the presented hyetographs (**Figures 4-6** and **Appendix B)**, actual rainfall distributions varied considerably between storms. It should be possible to characterize rainfall distribution types for individual storms, for example using mathematical approximations (Froehlich, 2009), and then to assess whether variations in intensity within storms affect *P* versus *Q* relationships. Having multiple years of data may be useful for capturing a range of relatively wet versus relatively dry years, and better quantify the role of antecedent moisture condition (AMC) in runoff processes. For example, using the AMC III category (representing the wettest antecedent conditions) provided the best match between modeled and measured runoff for catchments leading into a created wetland in Virginia during a rainy year (Fomchenko, 1998). While we are not directly measuring soil water content, we aim to evaluate different indices for antecedent moisture and incorporate remotely-sensed estimates of soil wetness into our analysis.

The anticipated final dataset from the project will include many more catchments than those analyzed in this preliminary report. This effort will include catchments that we are currently monitoring but were not included here because either i) we lacked a sufficient number of storms to perform the analyses or ii) our delineated catchment area was not accurate, and therefore will need to be re-scanned and re-analyzed once above-ground vegetated biomass is reduced. We are also in the process of generating similar data from other utility-scale solar sites, including several in which we are or will be monitoring runoff dynamics before, during, and eventually after construction. We anticipate adding 2-3 more sites to our study by the summer of 2026. Having this extended dataset will allow us to better quantify the variability in time lag parameters such as time of concentration and time of peak runoff within and between sites. As part of that assessment, we are measuring the orientation of solar panels using tilt sensors to measure the angles of solar panels relative to the ground surface. This information should help to assess whether panel orientation affects the apparent imperviousness of the panels.

Our stormwater quantity monitoring is being complemented by additional storm-specific water sampling and general site characterization. We are collecting stormwater samples from the study catchments during storms with at least 18 mm (0.75 inches) of anticipated accumulation, and are analyzing those samples for water quality parameters such as total phosphorus, total nitrogen, and total suspended solids. Finally, we are working with the site owners and operators to compile information used in the design of stormwater infrastructure in these catchments. With these data we will compare the parameters used in the design process (e.g., composite CNs) utilized for sizing stormwater BMPs versus the actual characteristics measured or inferred at each area.

5. References

Auerswald, K., & Gu, Q. L. (2021). Reassessment of the hydrologic soil group for runoff modelling. *Soil and Tillage Research*, *212*, 105034.

Bedient, P. B., Huber, W. C., & Vieux, B. E. (2019). *Hydrology and floodplain analysis*. 6th Edition. Pearson.

Chow, V. T., Maidment, D. R., & Mays, L. W. (1988). *Applied hydrology*. McGraw-Hill.

Dingman, S. L. (2015). *Physical hydrology*. 3rd Edition. Waveland Press.

Chin, D. A. (2017). Estimating the parameters of the curve number model. *Journal of Hydrologic Engineering*, *22*(6), 06017001.

Fomchenko, N. (1998). *Estimating the components of a wetland water budget* (M.S. thesis, Virginia Tech).

Froehlich, D. C. (2009). Mathematical formulations of NRCS 24-hour design storms. *Journal of irrigation and drainage engineering*, *135*(2), 241-247.

Hyland, E. (2025). *The changing landscape of energy generation in Virginia: How construction of utility-scale solar sites impacts soil physical and hydraulic properties* (M.S. thesis, Virginia Tech).

Kennedy, E.J. (1984). Discharge ratings at gaging stations. *U.S. Geological Survey Techniques of Water-Resources Investigations, Book 3*, Chapter A10, 59 p.

LIS (2022). HB 206 Small renewable energy projects; impact on natural resources, report. *Virginia's Legislative Information System (LIS), Division of Legislative Automated Systems*.

McCuen, R. H. (2009). Uncertainty analyses of watershed time parameters. *Journal of Hydrologic Engineering*, *14*(5), 490-498.

McPhillips, L., Buda, A., Easton, Z. Daniels, W. L., Fathel, S., Ignosh, J. Raj, C. & Sample, D. (2024). Best Management Practices to Minimize Impacts of Solar Farms on Landscape Hydrology and Water Quality. *STAC Publication Number 24-001*, Edgewater, MD. 42 p.

Moglen, G. E., Miller, J. J., & Cerrelli, G. (2025). Geographic Dependency of the Curve Number Method's Initial Abstraction Ratio. *Journal of Hydrologic Engineering*, *30*(4), 04025016.

U.S. Army Corps of Engineers (2023). *HEC-HMS Technical Reference Manual*. Hydrologic Engineering Center.

U.S. Department of Agriculture, Natural Resources Conservation Service. (1986). *Urban hydrology for small watersheds (TR-55)*. 2nd Edition. 162 p.

U.S. Department of Agriculture, NRCS (2021). Estimating Runoff Volume and Peak Discharge. *Part 650, Engineering Field Handbook. National Engineering Handbook*, Chapter 2, 36 p.

Walkowiak, D. K. (2006). *ISCO open channel flow measurement handbook*. 6th Edition. Teledyne ISCO. Lincoln, NE. 520 p.

Yin, S., Nearing, M. A., Borrelli, P., & Xue, X. (2017). Rainfall erosivity: An overview of methodologies and applications. *Vadose Zone Journal, 16*(12), 1-16.

Appendix A – Rating Curve Comparison

We used a rating curve equation provided by Teledyne ISCO to convert stage into discharge (Walkowiak, 2006):

$$q\ (cfs) = \ 2.23h^{2.31}$$

where h is water stage, h in ft and q is volumetric discharge, q (in cfs).

We compared the estimated values using this equation to tabular rating curve values provided by the United States Geological Survey (Kennedy, 1984), as shown in Figure A1.

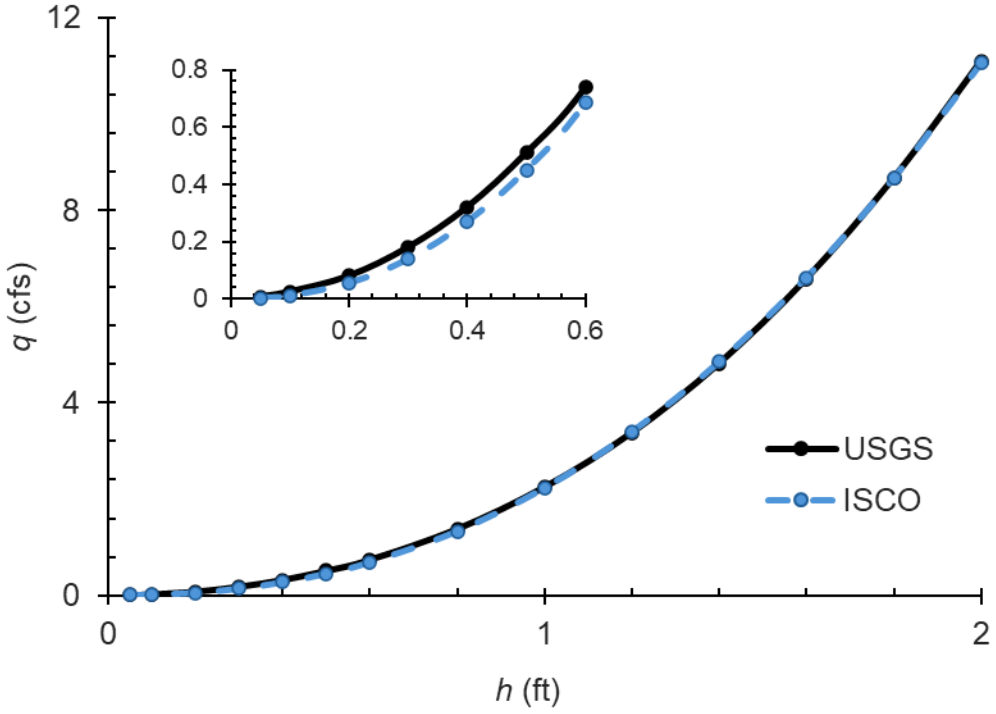

Figure A1. *Discharge (q, in cfs) versus stage (h, in ft) as estimated by the rating curve equation provided by Teledyne ISCO (ISCO) and the United States Geological Survey (USGS). The two curves had slight deviations at low stage (figure inset) but were nearly identical once h exceeded 1 ft.*

Appendix B – Determination of Effective Precipitation

We used an iterative fitting procedure to determine the value of ϕ (a uniform water loss rate) that created the best match between effective precipitation, P^* and total measured runoff, Q.

The initial abstraction, I_a, was calculated as the amount of precipitation that fell at the time of surface runoff initiation, t_{q0}:

$$I_a = \sum_{i=1}^{j} p_i \cdot \Delta t_i \quad \text{(C1)}$$

where p_i is the actual precipitation that fell in each timestep i, Δt_i is the length of each timestep, and j is the timestep associated with t_{q0}.

After t_{q0}, effective precipitation for each time step (p_i^*) was calculated as:

$$p_i^*(\phi) = \max(p_i - \phi \cdot \Delta t_i, 0) \quad \text{(C2).}$$

The total effective precipitation over the event, P^*, is:

$$P^* = \sum_{i=j}^{k} p_i^*(\phi) \quad \text{(C3)}$$

where k corresponds to the final timestep of measured precipitation.

We solved for the loss rate ϕ that makes the total effective rainfall, P^*, equal to the observed stormflow depth, Q:

$$P^* = Q \quad \text{(C4).}$$

To find the optimal ϕ, we used a bisection search between the lower (L) and upper bounds (U) for ϕ:

$$L = \phi_{\min}, \quad U = \phi_{\max} \quad \text{(C5)}$$

where the minimum possible loss rate, $\phi_{\min}$, was set to zero (no losses) and the maximum loss rate, $\phi_{\max}$, was set high enough that all rainfall is lost, ensuring the total effective rainfall becomes zero:

$$\phi_{\min} = 0 \quad \text{(C6)}$$

$$\phi_{\max} = \sum_i \left(\frac{\max(p_i, 0)}{\Delta t_i} \right) \quad \text{(C7).}$$

We then continued iterating until the estimated effective rainfall, $P^*(M)$, matched the observed Q within a small tolerance τ:

$$|P^*(M) - Q| < \tau \quad \text{(C8).}$$

For each iteration we computed the midpoint M between the current bounds:

$$M = \frac{L+U}{2} \quad \text{(C9).}$$

If the estimate was too high, our algorithm increased the loss rate by shifting *L* up, and if too low, it decreased the loss rate by shifting down *U* down, using the following criteria:

$$\text{If } F(M) > Q \text{ then set } L = M \quad \text{(C10a)}$$

$$\text{Else, set } U = M \quad \text{(C10b)}$$

The algorithm continued until determining the value of ϕ that best balanced rainfall and runoff:

$$\widehat{\phi} = M \quad \text{(C11)}$$

where $\widehat{\phi}$ is the final fitted water loss term (in mm/h).

Appendix C – Precipitation and Runoff Event Delineation

The identification of rainfall and runoff events required a number of approaches and parameters. An example set of hyetographs and hydrographs, along with corresponding timing metrics and threshold values, are shown in **Figures C1 – C5**.

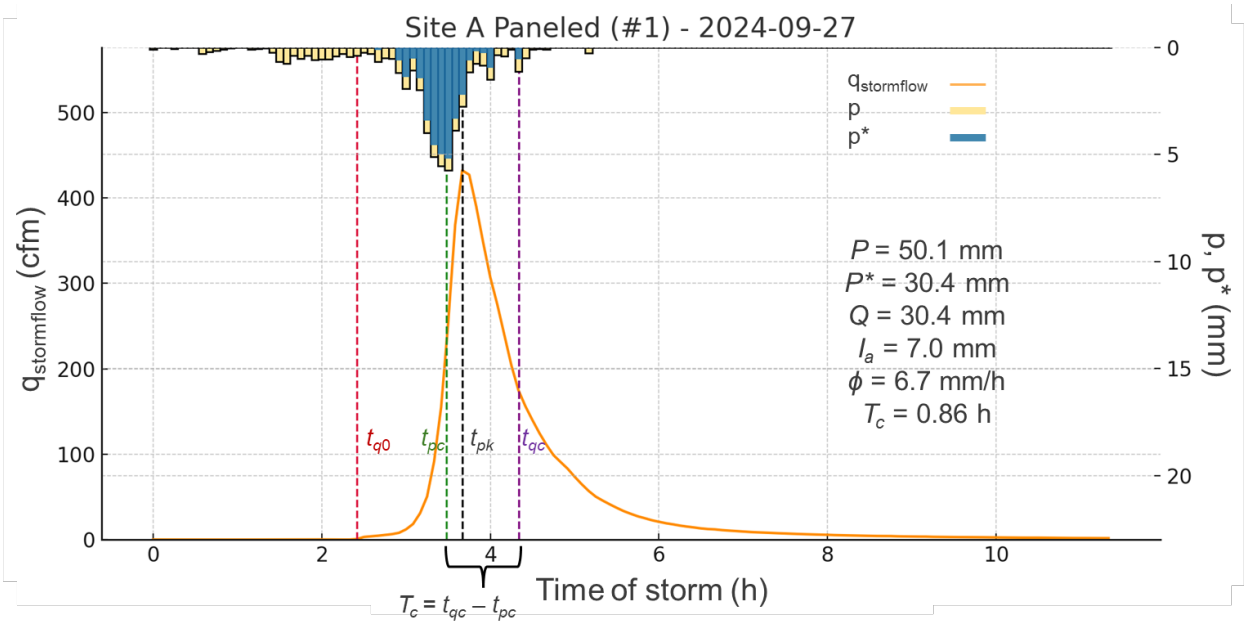

Figure C1*. An example hyetograph and hydrograph, showing measured precipitation (p), measured surface runoff ($q_{stormflow}$) and calculated effective precipitation (p*). The times indicated include: t_{q0} (start of surface runoff), t_{pc} (time of the centroid of the effective precipitation), t_{pk} (time of the hydrograph peak), t_{qc} (time of the centroid of the surface runoff), and T_c (time of concentration). P is the total amount of precipitation, P* is the total amount of effective precipitation, set to equal the total runoff Q, I_a is the initial abstraction, and ϕ is the calculated water loss rate. Data were collected from the solar catchment #1 in Site A, showing a storm that occurred on September 27, 2024.*

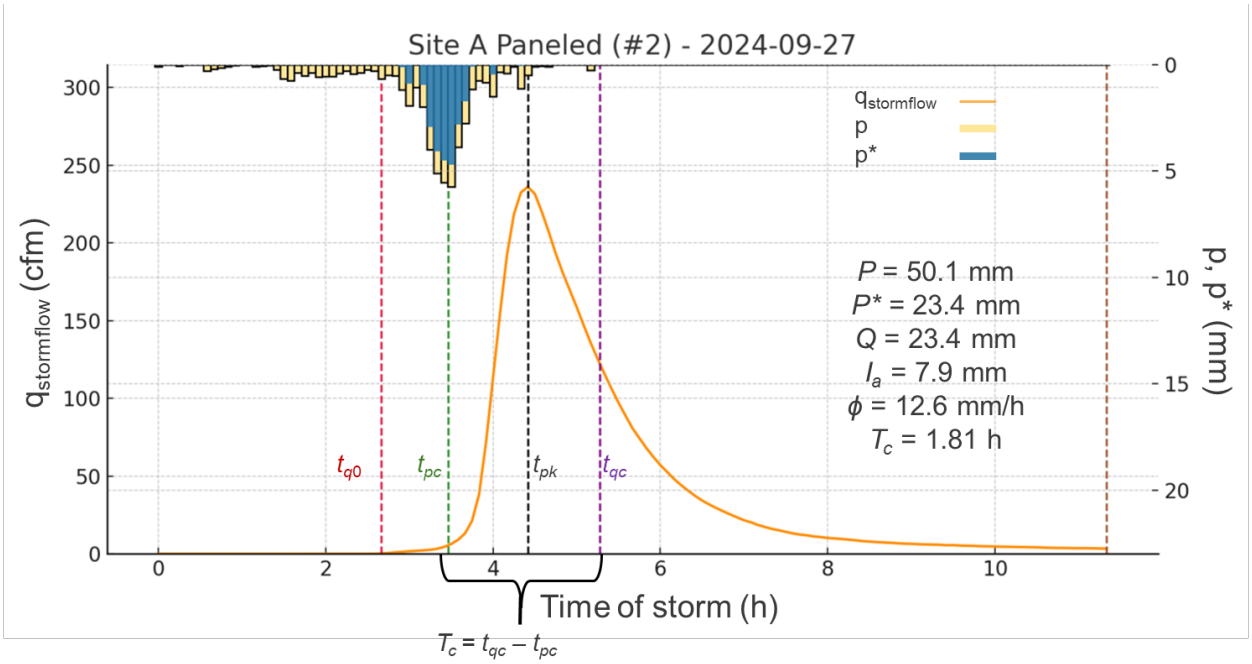

Figure C2. *An example hyetograph and hydrograph, showing measured precipitation (p), measured surface runoff ($q_{stormflow}$) and calculated effective precipitation (p*). The times indicated include: t_{q0} (start of surface runoff), t_{pc} (time of the centroid of the effective precipitation), t_{pk} (time of the hydrograph peak), t_{qc} (time of the centroid of the surface runoff), and T_c (time of concentration). P is the total amount of precipitation, P* is the total amount of effective precipitation, set to equal the total runoff Q, I_a is the initial abstraction, and ϕ is the calculated water loss rate. Data were collected from the solar catchment #2 in Site A, showing a storm that occurred on September 27, 2024.*

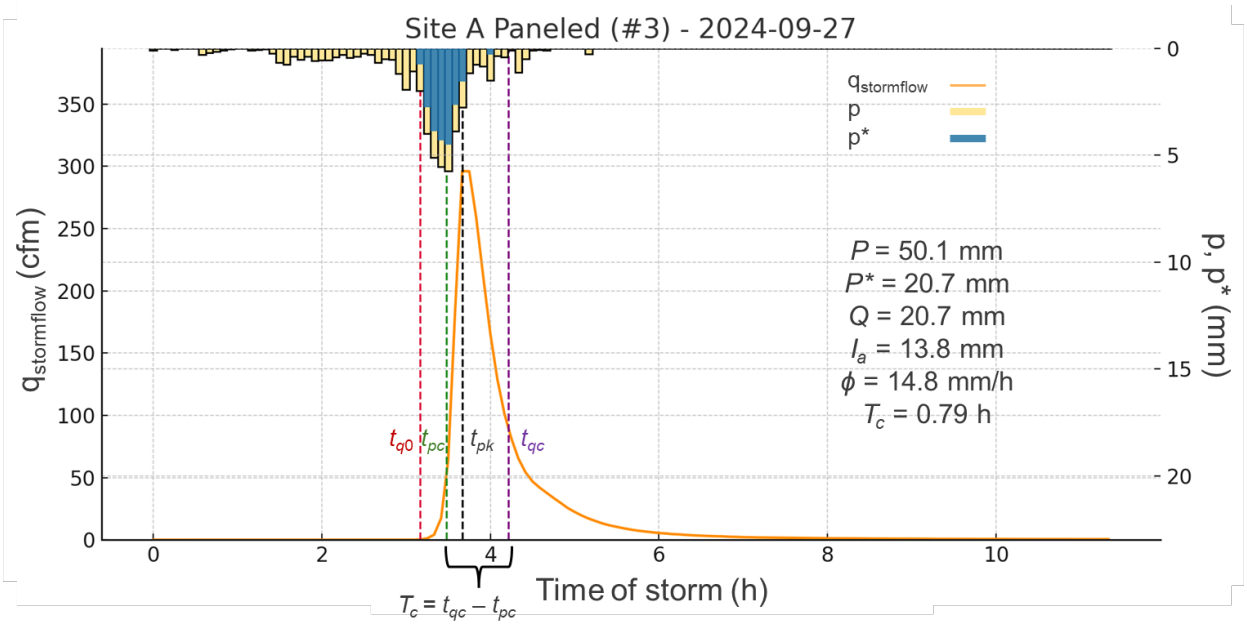

Figure C3. *An example hyetograph and hydrograph, showing measured precipitation (p), measured surface runoff ($q_{stormflow}$) and calculated effective precipitation (p*). The times indicated include: t_{q0} (start of surface runoff), t_{pc} (time of the centroid of the effective precipitation), t_{pk} (time of the hydrograph peak), t_{qc} (time of the centroid of the surface runoff), and T_c (time of concentration). P is the total amount of precipitation, P* is the total amount of effective precipitation, set to equal the total runoff Q, I_a is the initial abstraction, and ϕ is the calculated water loss rate. Data collected from the solar catchment #3 in Site A, showing a storm that occurred on September 27, 2024.*

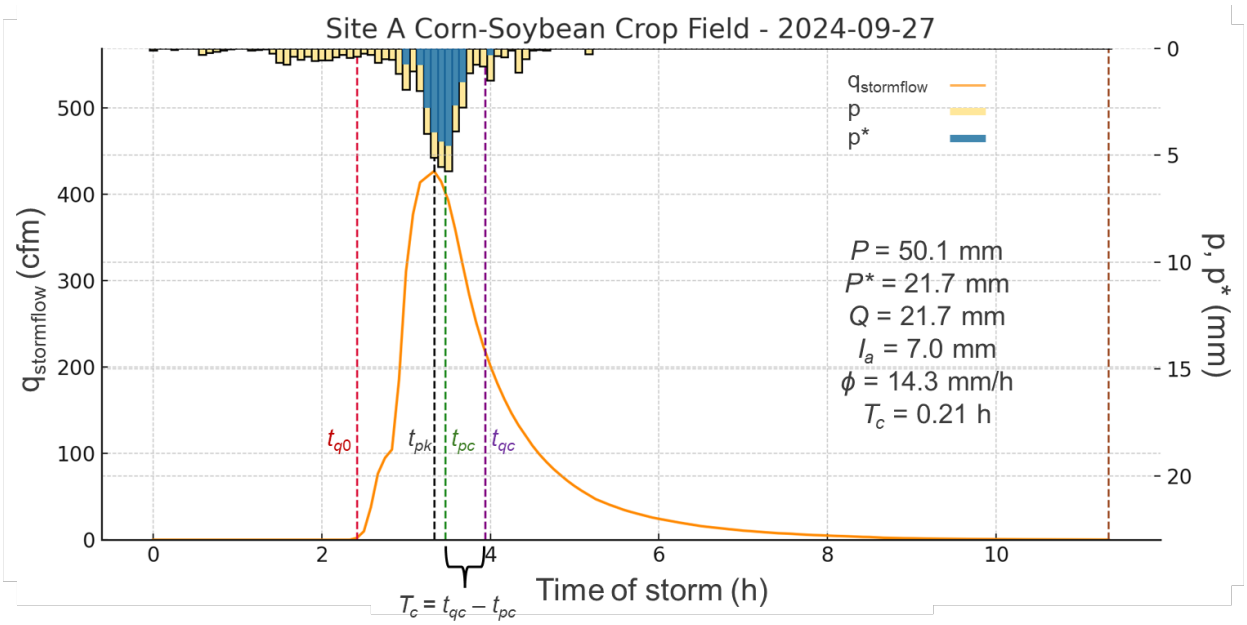

Figure C4. *An example hyetograph and hydrograph, showing measured precipitation (p), measured surface runoff ($q_{stormflow}$) and calculated effective precipitation (p*). The times indicated include: t_{q0} (start of surface runoff), t_{pc} (time of the centroid of the effective precipitation), t_{pk} (time of the hydrograph peak), t_{qc} (time of the centroid of the surface runoff), and T_c (time of concentration). P is the total amount of precipitation, P* is the total amount of effective precipitation, set to equal the total runoff Q, I_a is the initial abstraction, and ϕ is the calculated water loss rate. Data collected from the corn-soybean catchment in Site A, showing a storm that occurred on September 27, 2024.*

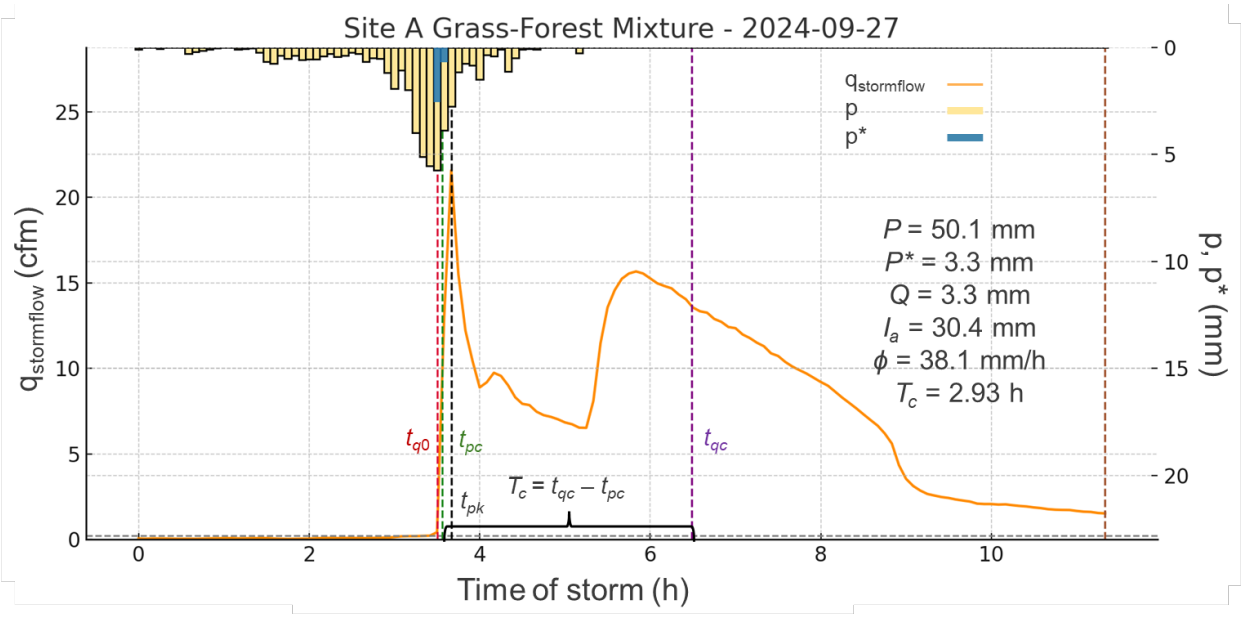

Figure C5. *An example hyetograph and hydrograph, showing measured precipitation (p), measured surface runoff ($q_{stormflow}$) and calculated effective precipitation (p*). The times indicated include: t_{q0} (start of surface runoff), t_{pc} (time of the centroid of the effective precipitation), t_{pk} (time of the hydrograph peak), t_{qc} (time of the centroid of the surface runoff), and T_c (time of concentration). P is the total amount of precipitation, P* is the total amount of effective precipitation, set to equal the total runoff Q, I_a is the initial abstraction, and ϕ is the calculated water loss rate. Data collected from the grass-forest catchment in Site A, showing a storm that occurred on September 27, 2024.*

Appendix D – Apparent CNs for Site C

This appendix presents measured *P* and *Q* data from three catchments in Site C that have been developed with solar panels. The CN model was fit to the observed data assuming the initial abstraction $\lambda = 0.20$ (**Figures D1 – D3**). We have not collected sufficient observations from reference catchments at this site, so we are not yet able to make direct comparisons here.

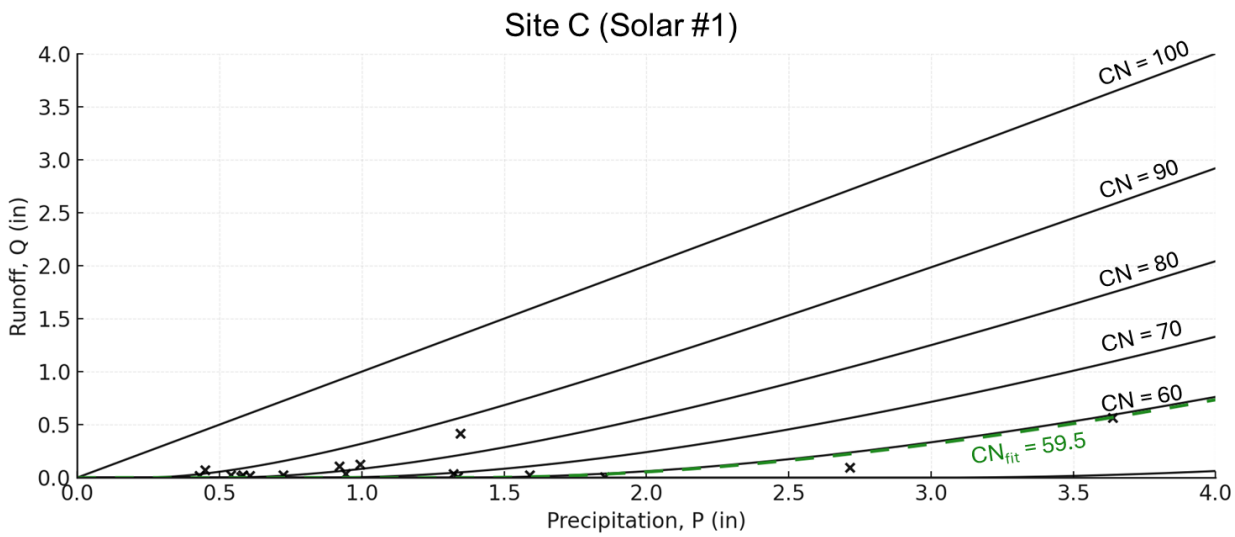

***Figure D1**. Precipitation (P) and runoff (Q) for different storms measured at Site C in a catchment developed with solar panels (points), along with the P-Q relationships modeled by different curve number (CN) values assuming initial abstraction $\lambda = 0.20$ (solid lines). The dashed green line indicates the CN value that best fits the top 50% of storms (by relative runoff) using least-squares regression.*

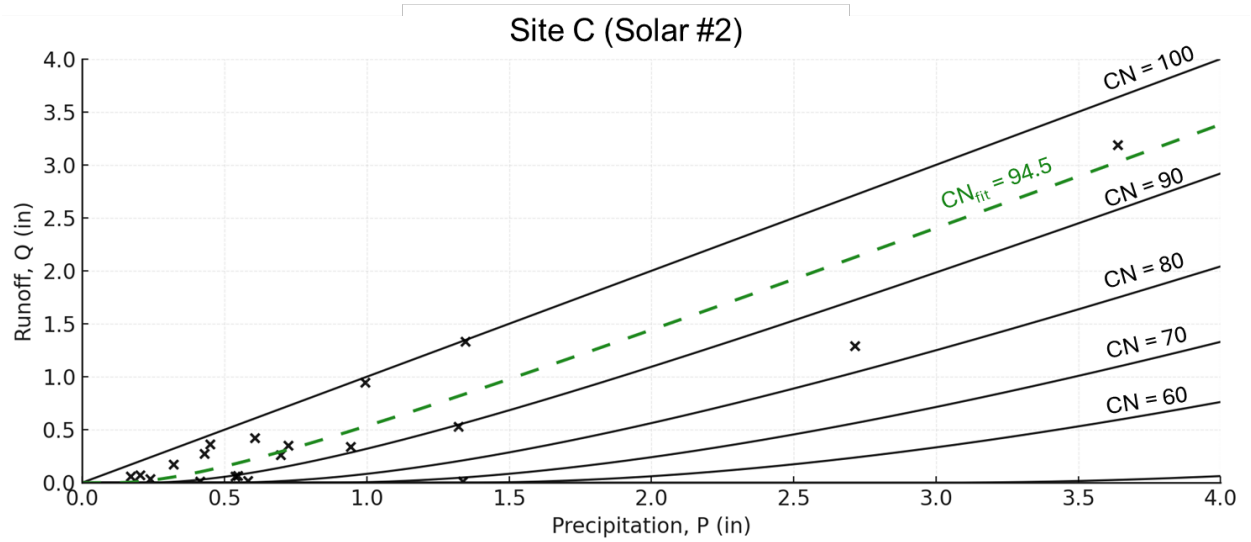

Figure D2. *Precipitation (P) and runoff (Q) for different storms measured at Site C in a catchment developed with solar panels (points), along with the P-Q relationships modeled by different curve number (CN) values assuming initial abstraction λ = 0.20 (solid lines). The dashed green line indicates the CN value that best fits the top 50% of storms (by relative runoff) using least-squares regression.*

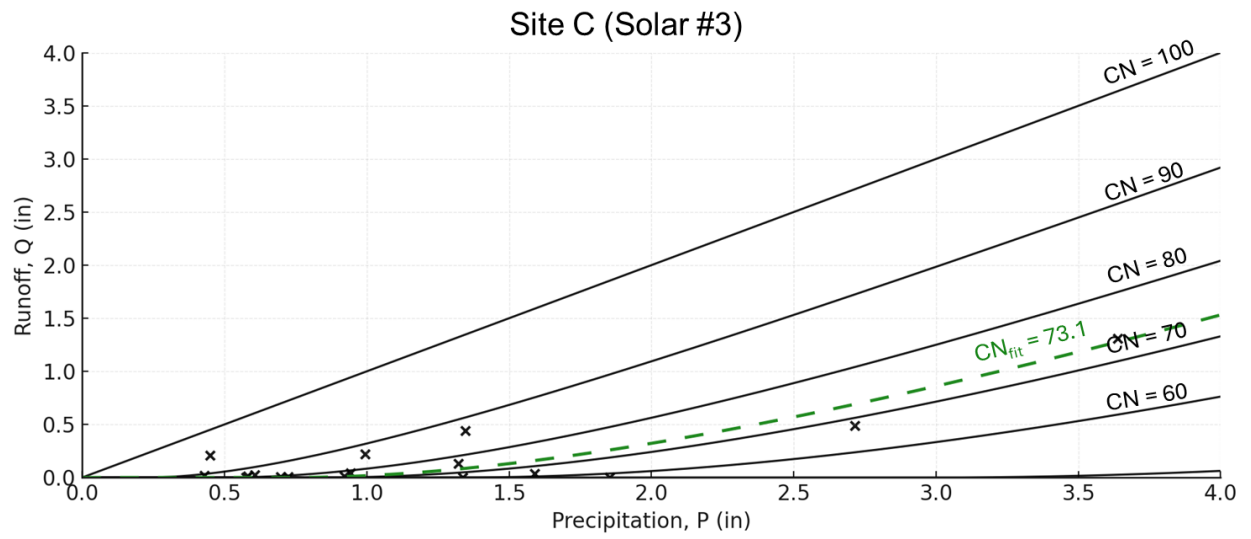

Figure D3. *Precipitation (P) and runoff (Q) for different storms measured at Site C in a catchment developed with solar panels (points), along with the P-Q relationships modeled by different curve number (CN) values assuming initial abstraction λ = 0.20 (solid lines). The dashed green line indicates the CN value that best fits the top 50% of storms (by relative runoff) using least-squares regression.*

Appendix E – Apparent CNs assuming Initial Abstraction Ratio λ = 0.05

This appendix presents measured *P* and Q data from the three sites, along with modeled CN isolines and best fit CN for each site, all generated assuming that the initial abstraction ratio value $\lambda = 0.05$ (**Figures E1 – E11**).

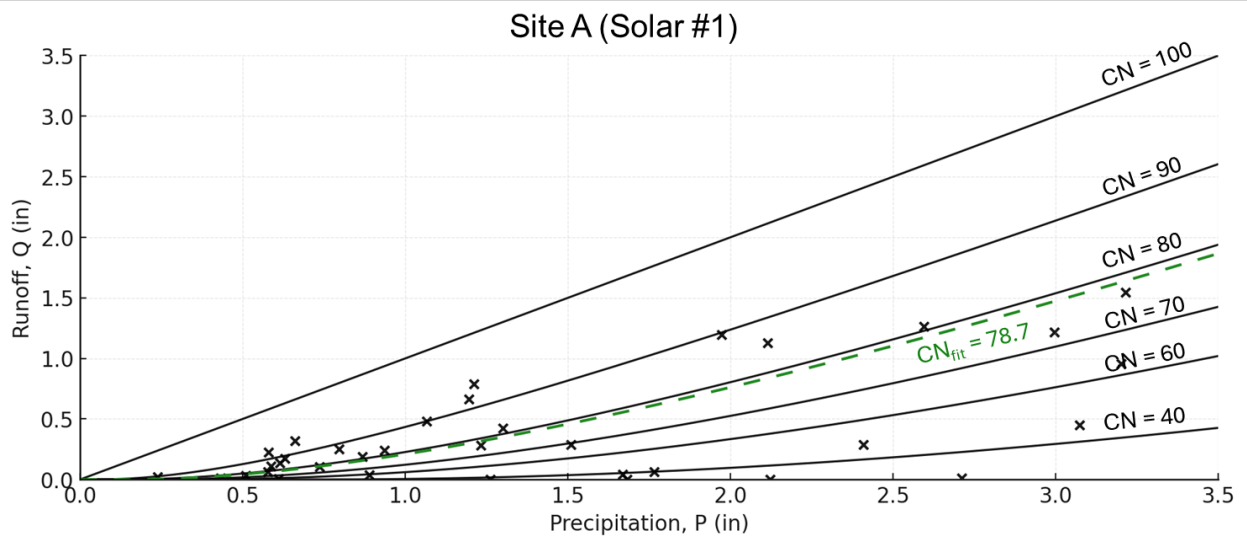

Figure E1*. Precipitation (P) and runoff (Q) for different storms measured at Site A in a catchment developed with solar panels (points), along with the P-Q relationships modeled by different curve number (CN) values assuming initial abstraction λ = 0.05 (solid lines). The dashed green line indicates the CN value that best fits the top 50% of storms (by relative runoff) using least-squares regression.*

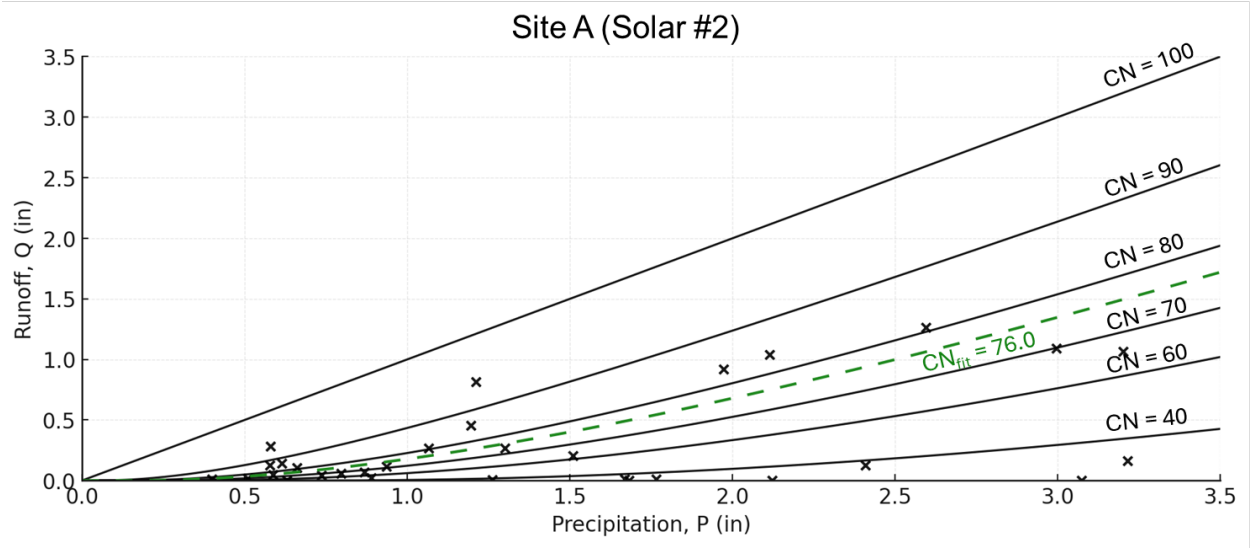

Figure E2. *Precipitation (P) and runoff (Q) for different storms measured at Site A in a catchment developed with solar panels (points), along with the P-Q relationships modeled by different curve number (CN) values assuming initial abstraction λ = 0.05 (solid lines). The dashed green line indicates the CN value that best fits the top 50% of storms (by relative runoff) using least-squares regression.*

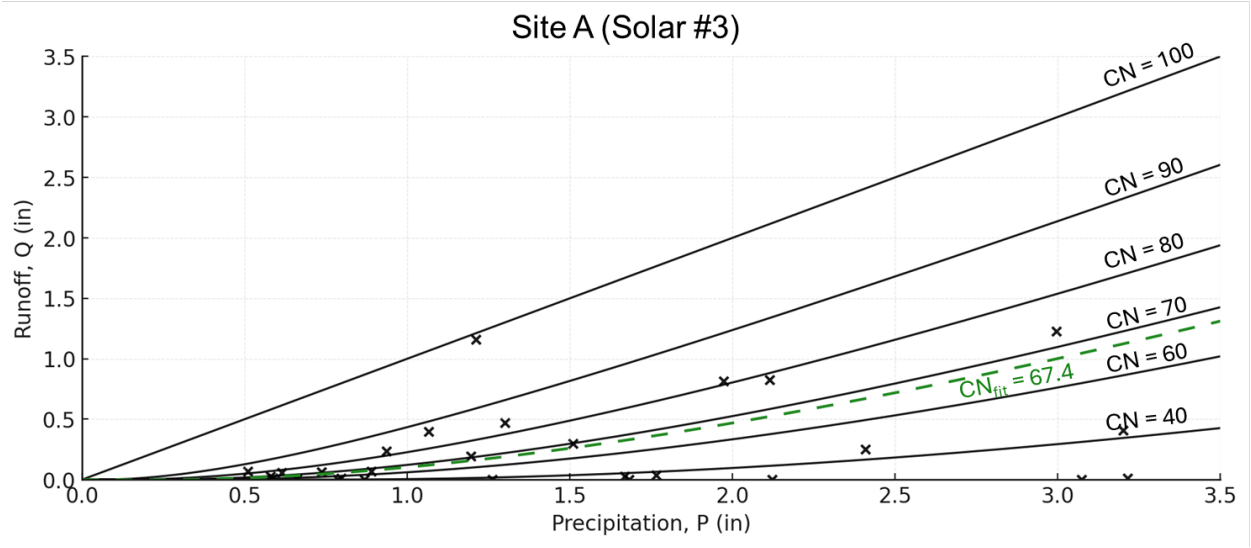

Figure E3. *Precipitation (P) and runoff (Q) for different storms measured at Site A in a catchment developed with solar panels (points), along with the P-Q relationships modeled by different curve number (CN) values assuming initial abstraction λ = 0.05 (solid lines). The dashed green line indicates the CN value that best fits the top 50% of storms (by relative runoff) using least-squares regression.*

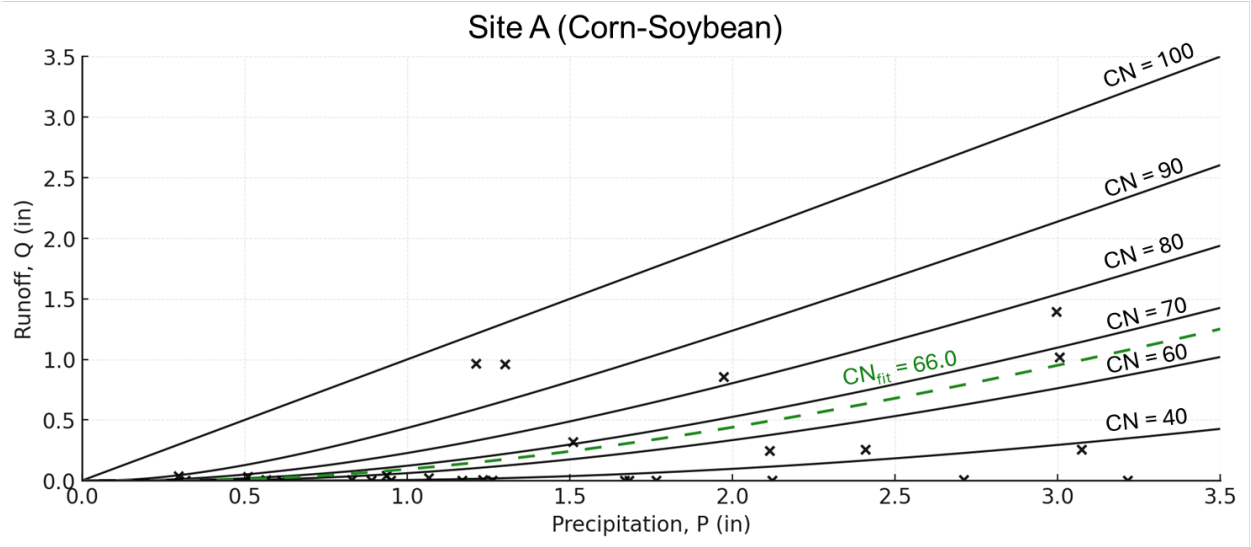

Figure E4. *Precipitation (P) and runoff (Q) for different storms measured at Site A in a reference catchment planted in a corn-soybean rotation (points), along with the P-Q relationships modeled by different curve number (CN) values assuming initial abstraction λ = 0.05 (solid lines). The dashed green line indicates the CN value that best fits the top 50% of storms (by relative runoff) using least-squares regression.*

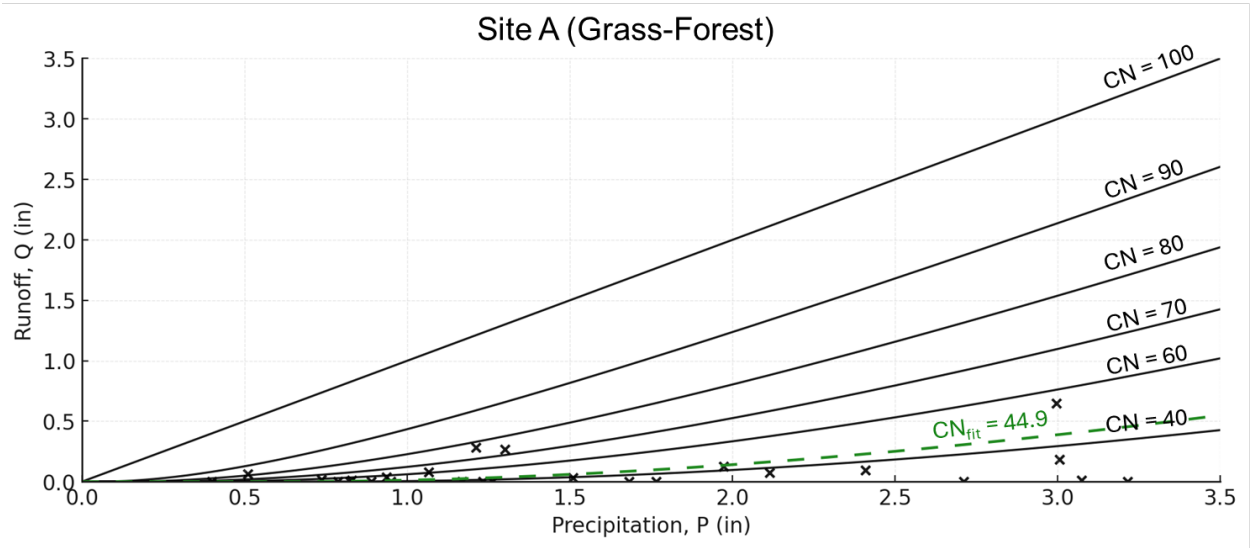

Figure E5. *Precipitation (P) and runoff (Q) for different storms measured at Site A in a reference catchment characterized by mixed grass and forest (points), along with the P-Q relationships modeled by different curve number (CN) values assuming initial abstraction λ = 0.05 (solid lines). The dashed green line indicates the CN value that best fits the top 50% of storms (by relative runoff) using least-squares regression.*

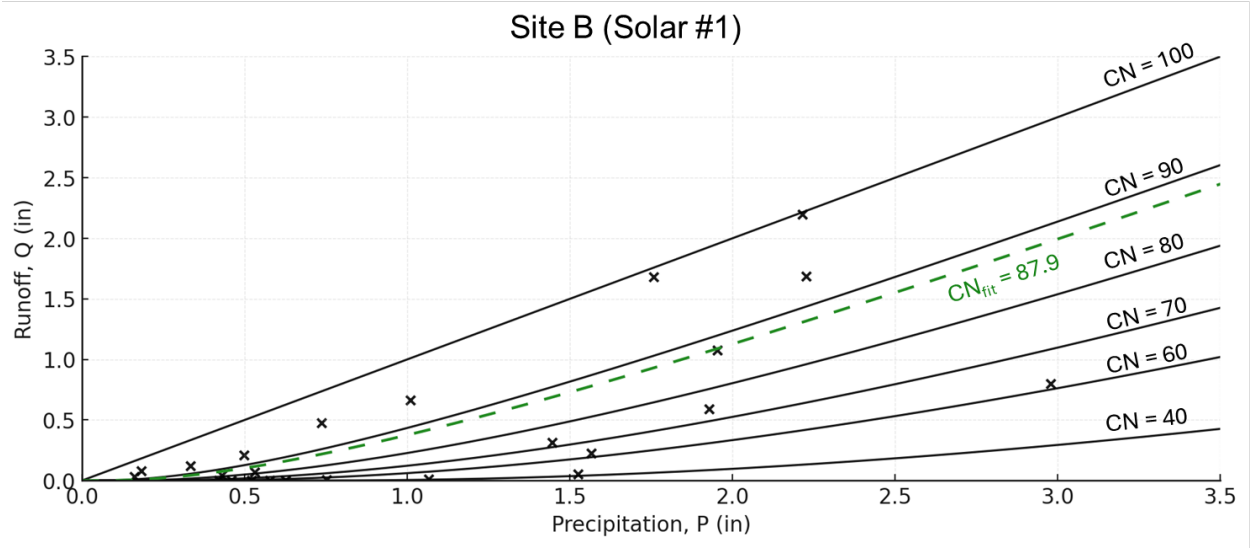

***Figure E6**. Precipitation (P) and runoff (Q) for different storms measured at Site A in a catchment with a mixture of grassy and forested areas (points), along with the P-Q relationships modeled by different curve number (CN) values assuming initial abstraction $\lambda = 0.05$ (solid lines). The dashed green line indicates the CN value that best fits the top 50% of storms (by relative runoff) using least-squares regression.*

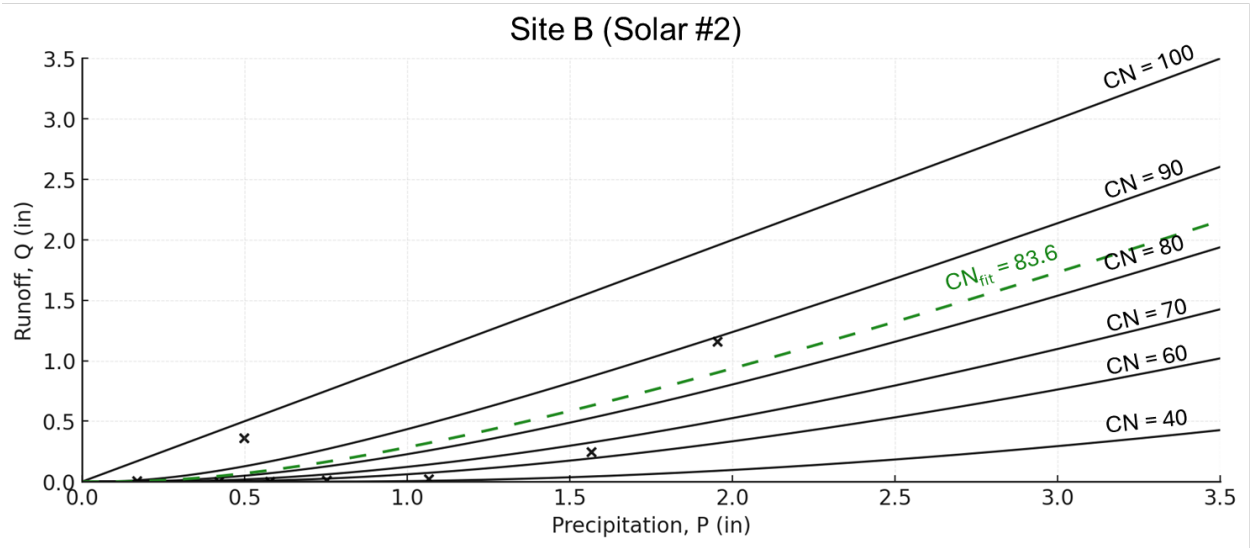

***Figure E7**. Precipitation (P) and runoff (Q) for different storms measured at Site B in a catchment developed with solar panels (points), along with the P-Q relationships modeled by different curve number (CN) values assuming initial abstraction $\lambda = 0.05$ (solid lines). The dashed green line indicates the CN value that best fits the top 50% of storms (by relative runoff) using least-squares regression.*

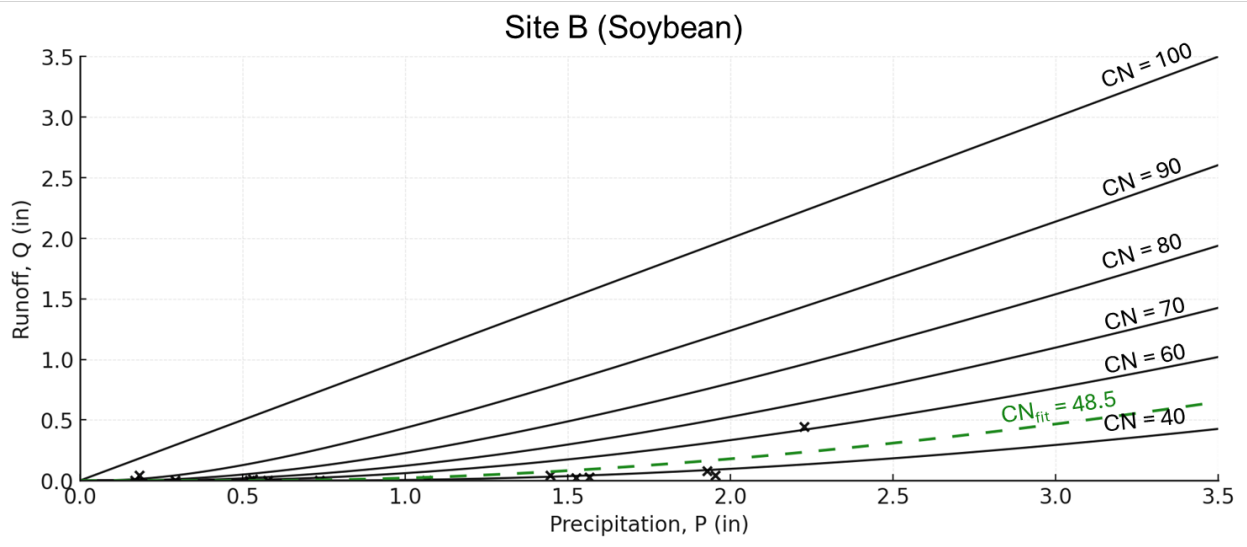

Figure E8. *Precipitation (P) and runoff (Q) for different storms measured at Site B in a reference catchment draining from a soybean field (points), along with the P-Q relationships modeled by different curve number (CN) values assuming initial abstraction $\lambda = 0.05$ (solid lines). The dashed green line indicates the CN value that best fits the top 50% of storms (by relative runoff) using least-squares regression.*

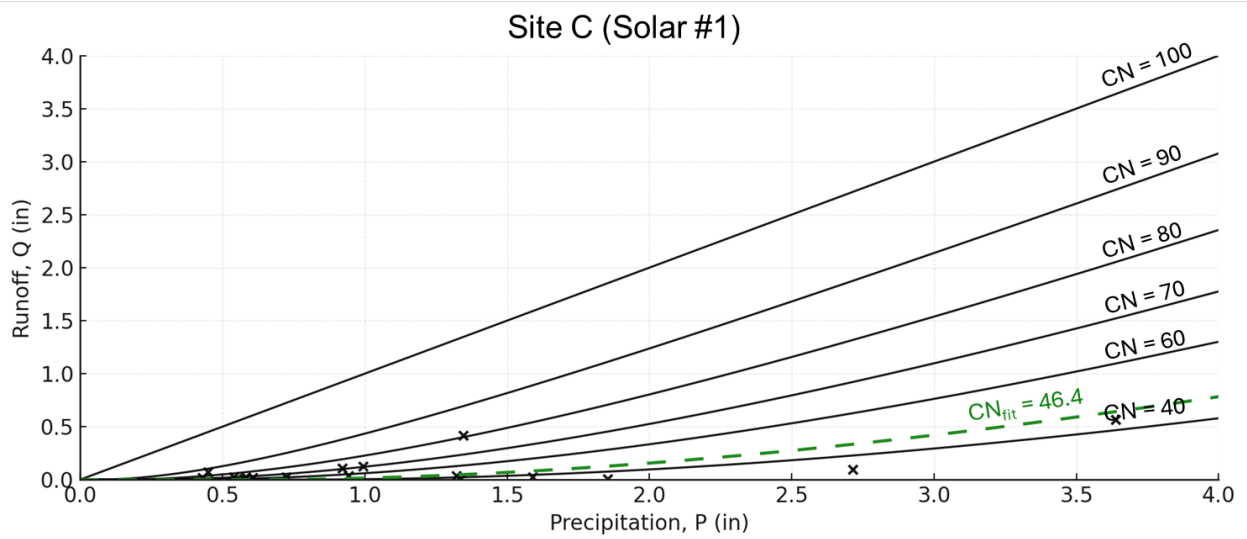

Figure E9. *Precipitation (P) and runoff (Q) for different storms measured at Site C in a catchment developed with solar panels (points), along with the P-Q relationships modeled by different curve number (CN) values assuming initial abstraction $\lambda = 0.05$ (solid lines). The dashed green line indicates the CN value that best fits the top 50% of storms (by relative runoff) using least-squares regression.*

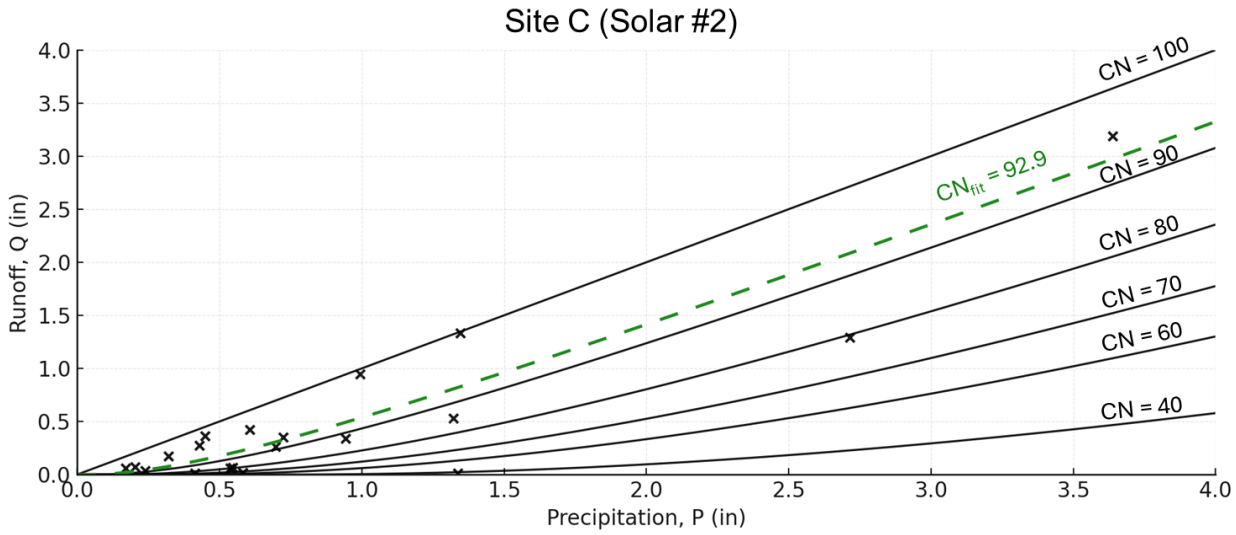

Figure E10. *Precipitation (P) and runoff (Q) for different storms measured at Site C in a catchment developed with solar panels (points), along with the P-Q relationships modeled by different curve number (CN) values assuming initial abstraction λ = 0.05 (solid lines). The dashed green line indicates the CN value that best fits the top 50% of storms (by relative runoff) using least-squares regression.*

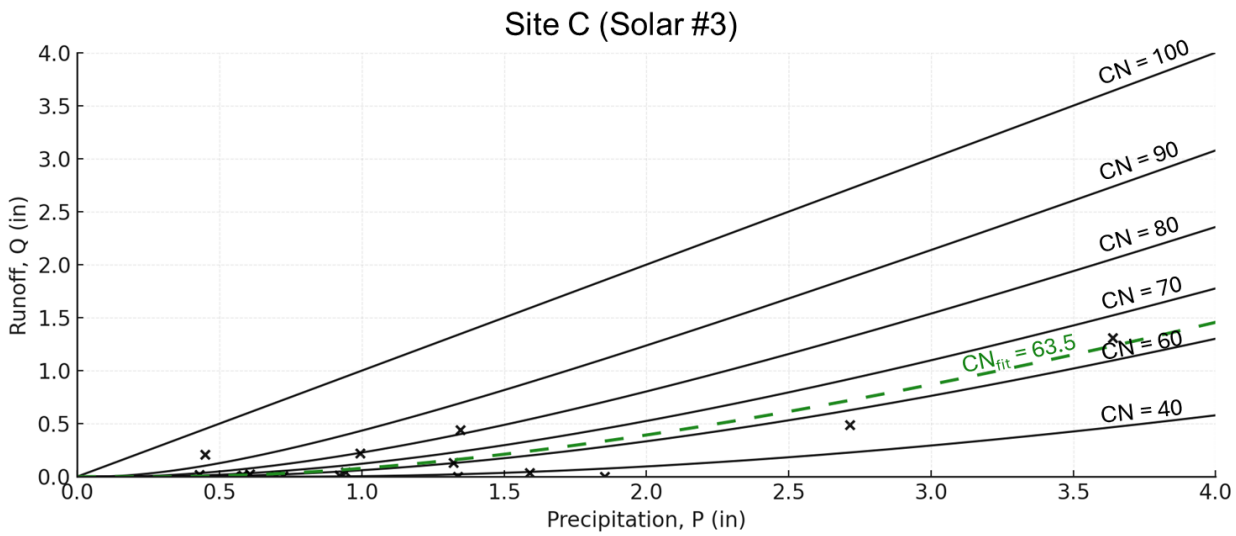

Figure E11. *Precipitation (P) and runoff (Q) for different storms measured at Site C in a catchment developed with solar panels (points), along with the P-Q relationships modeled by different curve number (CN) values assuming initial abstraction λ = 0.05 (solid lines). The dashed green line indicates the CN value that best fits the top 50% of storms (by relative runoff) using least-squares regression.*